



POLITECNICO
MILANO 1863

**SCUOLA DI INGEGNERIA INDUSTRIALE
E DELL'INFORMAZIONE**

EXECUTIVE SUMMARY OF THE THESIS

Analysis and compensation of friction in the TWIN lower-limb exoskeleton: a model-based approach

LAUREA MAGISTRALE IN BIOMEDICAL ENGINEERING - INGEGNERIA BIOMEDICA

Author: ALESSIA SACCHINI

Advisor: PROF. ELENA DE MOMI

Co-advisors: FEDERICO TESSARI, STEFANO MALUDROTTU, CHRISTIAN VASSALLO

Academic year: 2020-2021

1. Introduction

Due to traumatic events or special medical conditions, a large number of individuals worldwide are affected by motor impairment. The World Health Organisation statistics state that every year, around the world, between 250 000 and 500 000 people suffer a spinal cord injury (SCI) and 15 million people suffer a stroke. Of these, 5 million die and another 5 million are left permanently disabled, placing a burden on family and community [1]. For these patients, neuro-motor rehabilitation is an effective therapy that aims to promote the patient's abilities and attempt to make them as independent as possible. In this context it is possible to find rehabilitative exoskeletons, electromechanical devices capable of supporting (partially or totally) the weight of the patient's body and replace or enhance his movement. They also can measure with objectivity, repeatability and precision different parameters (kinematic and dynamic ones) of movement, due to the presence of appropriate sensors in their structure. This makes possible an accurate and quantitative assessment of motor function that allows to better plan the therapeutic path [2]. However, it should be kept in mind that in order to have clinical benefit, exoskele-

tons should:

- adapt to the needs of the patient by varying the level of assistance according to the type and severity of the disability (at the limit, ability to work in total transparency);
- be capable of providing appropriate sensory input and feedback information to the patient;
- allow for variations in external exercise conditions and be fairly compliant with the patient's voluntary movement.

Therefore, it is very important for an exoskeleton to be able to work in transparency and to be able to adjust it gradually according to the stage of the rehabilitation process. A lack in transparency in fact can generate undesired resistances during the motion of patients. In other terms, the exoskeleton has to be possibly "transparent" to the patient and this can be achieved with an adequate friction compensation.

Moreover, the robot should provide active and adaptive assistance (*Assist as needed* approach). With an AAN control strategy, the device contribution to movement is based on the patient's effort and physical condition. This solution promotes patients intention, motivation, encouraging them to trigger the exoskeleton assistance

by their own active effort [3]. A very effective solution to get a compliant active exoskeleton controller, is to use force interaction controllers, mostly used in form of either the impedance or admittance controllers. These controllers in fact are able to reduce or possibly zero the interaction force of the human-exoskeleton system. Nowadays, more and more exoskeletons control the interaction forces by using impedance control algorithms [4].

In this work we present a sensorless methodology to create a model for friction compensation and a preliminary design of a model-based impedance controller for the TWIN lower-limb exoskeleton [5]. In Section 2 after a description of the TWIN structure, the experimental setup is explained. Results of the testing campaign are analyzed to build the model in Section 2.3 and the impedance control in Section 2.4. The validation of this work is discussed in Section 3. Section 4 shows our conclusions and future works.



Figure 1: The TWIN lower-limb exoskeleton worn by a patient.

2. Methodology

TWIN is a powered lower-limb exoskeleton developed at the IIT-INAIL Rehab Technologies Lab. TWIN is designed for people with spinal cord injury or stroke. Its structure provides the control of the knee and hip joints by means of four motors and five rigid sections: a pelvis and two separate components, for each leg, of the femur and tibia. The distinctive feature of this exoskeleton is its complete modularity: the exoskeleton can be disassembled by the user into small sub-units without the need of additional tools, so as to facilitate its management, don-

ning and transportation [5]. During its use, the use of a walking aid, such as crutches or a walker, is mandatory as shown in Figure 1.

2.1. Test bench

This thesis project aims first of all to carry out a friction analysis of TWIN, therefore the exoskeleton is separated into its fundamental parts: the joints. The idea is to start from a TWIN joint, see which losses act on it and then quantify them. In order to do this, an ad hoc test bench was built, as shown in Figure 2a.

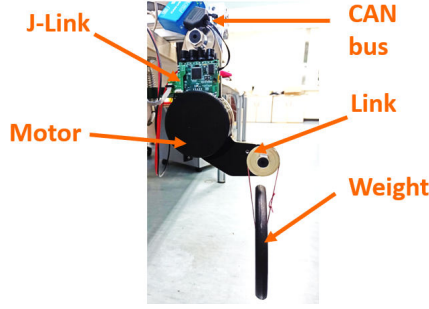
The test bench is powered by a high power Lithium Ion Smart Battery (CMX820P). The electrical energy is then transformed into torque through a brushless DC motor. Also an inverter DRV8301 is present in order to mix the input electrical quantities from the power supply and transform them appropriately to drive the electric motor. The motors employed for the knee and hip have different nominal voltages, 24V and 36V, respectively, to meet the different torque/speed requirements of these two joints. Also an encoder is present in order to perform the position control. The motor is actuated by a logic board based on an ARM Cortex M4 microcontroller unit. A fundamental element is the transmission unit that is characterized by the transmission ratio τ , which in our case is equal to 1:100. In the joint the Harmonic Drive (HD), model CSD-25-100-2A-GR-BB, is used. The joint was then connected to the PC, a Dell XPS 15, and the communication between the two was via a JTAG cable and CAN bus. From the PC, through the user graphic interface, it is possible to select the type of joint and therefore the motor used, but also the kind of controller to activate. After the joint has been moved for some tests and once the control is disabled, it is possible to measure position, current, voltage bus, velocity and duty.

2.2. Analysis of friction

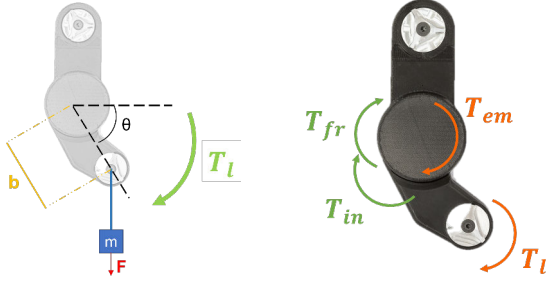
A testing campaign was carried out with the aim of analyzing the torques acting on the joints. The tests were performed by attaching different weights (3kg, 2.5kg, 2kg, 1.5kg, 1kg) to the joint's rigid link, as shown in Figure 2a and the controller employed was a duty-based transparency control.

The transparency measures the robot ability of

not applying any assistance/resistance to free motion. So enabling the duty-based transparency control and setting the rigid link to an initial known position with the weight attached, the link lowers until it reaches the stop (the link is stopped by a mechanical stop that avoid hyper-extension).



(a) TWIN's joint and the main elements of the test bench.



(b) Load torque acting on the joint.

(c) Joint' torques.

Figure 2: TWIN joint. The figure (a) represents the test bench used to carry out the tests. The figure (b) shows the weight force and the resulting load torque, while the figure (c) shows all the torque contributions: the orange arrows are the load and electromechanical torques, the green ones are the dissipation torques.

Knowing therefore the weight force F , the link's length b , the variation of position θ thanks to the encoder (see Figure 2b), it is possible to find the load torque simply by multiplying the lever arm by the force, as expressed by the equation (1).

$$T_l = F \cdot b \cos\theta \quad (1)$$

After extracting from the tests output files the vectors for time and position, the load torque for each weight was computed according to equation (1).

In addition to load torque, also electromechanical torque has an effect on the joint and is com-

puted according to the following equation:

$$T_{em} = K_t \tau \cdot I \quad (2)$$

where K_t is the constant factor motor torque (known from the motor data-sheet) and I is the motor current and is given by tests output files. Regarding the losses acting on the joint, these are the inertia and friction torques as illustrated in Figure 2c.

The inertial torque is computed as follows: .

$$\begin{aligned} T_{in} &= J_{system} \cdot \dot{\omega} = \\ &= [J_{motor} \cdot \tau^2 + J_{gearbox} + \\ &\quad + J_{link} + J_{mass}] \cdot \dot{\omega} \quad (3) \end{aligned}$$

where J_{system} is the inertia of the system, hence of the motor-harmonic drive system and load. J_{motor} and $J_{gearbox}$ values can be found in the data-sheet of the motor and the harmonic drive, J_{link} can be derived from the CAD of the joint, while $J_{mass} = m \cdot b^2$.

The angular acceleration $\dot{\omega}$ instead is computed deriving twice the angular position θ . However, this operation created a noisy signal with a frequency of 1000Hz that was filtered first with a downsampling of 10 and then with a moving average filter with a window size of 10. At this point it is possible to obtain the friction torque through the dynamic equilibrium equation for the system (Newton's Law): .

$$\begin{aligned} T_{fr} &= K_t \tau \cdot I + F \cdot b \cos\theta + \\ &\quad - [J_{motor} \cdot \tau^2 + J_{gearbox} + J_{link} + \\ &\quad + J_{mass}] \cdot \dot{\omega} \quad (4) \end{aligned}$$

2.3. Friction model

The friction torque for each weight was computed according to equation (4) and then all the results were imported in the Curve Fitting Toolbox of MATLAB in order to create a model that fits all the data. The model chosen to represent the knee joint's friction is the *rotational friction*, so a model that takes into account the contribution of Coulomb+viscous friction, but also the Stribeck effect. This choice had already been hypothesized by the study of the literature and then it was also confirmed experimentally on the basis of the results obtained from the testing campaign.

So, it turns out that the friction torque data collected are represented by the following model:

$$T_{fr} = \sqrt{2}e(a-b) \cdot e^{\left(\frac{\omega}{c\sqrt{2}}\right)^2} \cdot \frac{\omega}{c\sqrt{2}} + b \cdot \tanh\left(\frac{\omega}{c/10}\right) + d\omega \quad (5)$$

where a, b, c, d are parameters generated by the toolbox. The first term, exponential, is the Stribeck contribution; the second term represents the static friction and is given by the coefficient of static friction b , multiplied by a hyperbolic tangent, whose peculiar trend avoids singularities at the origin; the last term instead represents the viscous friction and is given by the coefficient of viscous friction d , multiplied by the angular velocity ω , i.e. $\dot{\theta}$. The model for the hip joint was generated in the same manner, changing parameters a, b, c, d appropriately. Once the friction model has been found for each joint, it needs to be tested. The implementation of the model goes through three sub-stages:

1. implementation on the TWIN's firmware of the filtering method;
2. inserting the model (5) in the firmware, within a torque control. This control in fact is suitable for our application because computes the target current dividing the total acting torque by $K_t \cdot \tau$. Moreover a gain parameter G has been introduced to regulate the compensation percentage, as expressed by the equation (6);
3. configuration of the torque control within the TWIN's software.

$$I = \frac{1}{K_t \tau} [T_{in} + T_{fr} \cdot G] \quad (6)$$

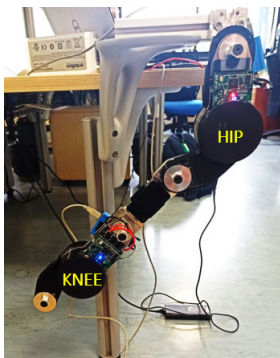


Figure 3: Hip-femur-knee test bench: the elements are the same of the single joint test bench, but two CAN bus are used.

At this point, the hip and knee joints were physically connected via a link, representing the femur (see Figure 3), to perform tests on the entire leg and to verify that the models created would also work on a test bench of greater complexity.

2.4. Impedance control

Friction compensation is performed employing the torque controller, in which it was also possible to realize a preliminary design for an impedance control. The concept of impedance control in the field of robotics has been introduced by Hogan [6]. Impedance control aims in particular to ensure that the manipulator (the joint in the case of the exoskeleton), controlled in position and in interaction with the environment, manifests the behavior of an impedance, assimilated to a generalized mass-spring-damper system.

In TWIN we implemented this kind of control. Thanks to the encoder, in fact, the position values are known instant by instant. A description of this controller is in Figure 4.

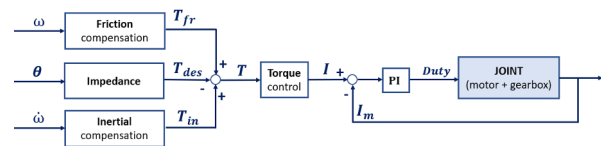


Figure 4: TWIN impedance controller diagram: the exoskeleton is capable of measuring θ actuator positions and imparting a desired torque through an impedance control. Then the torque controller, given also the friction torque and the inertial torque, computes the motor current to drive the joint. The diagram shows how the motor current is controlled by a PI controller, that takes the $(I - I_m)$ signal as input where I_m is the measured current.

For simplicity and to verify that this control actually works, only the contribution of the spring was considered, so the torque T_{des} is directly proportional to θ position by a factor of k , i.e., a stiffness.

$$T_{des} = k \cdot (\theta - \theta_0) \quad (7)$$

This means that when the joint moves away from its initial position, exactly as happens in a spring, a recall torque is exerted proportional to the displacement from the initial position, according to the stiffness. Once the initial position θ_0 and k have been chosen, the torque contribution has been implemented in the torque con-

troller, in the following way: .

$$I = \frac{1}{K_t \tau} [T_{in} + T_{fr} \cdot G - T_{des}] \quad (8)$$

where T_{des} is the impedance torque. The last step of the thesis project, included the implementation of the impedance control on the whole leg (hip-femur-knee test bench in Figure 3).

3. Results and discussion

3.1. Friction model

The results of the friction torques fitting are in Figure 5, where the friction torque T_{fr} over the angular velocity is illustrated. The two models of hip and knee joints are almost superimposed and differ only for the Stribeck and Coulomb effects.

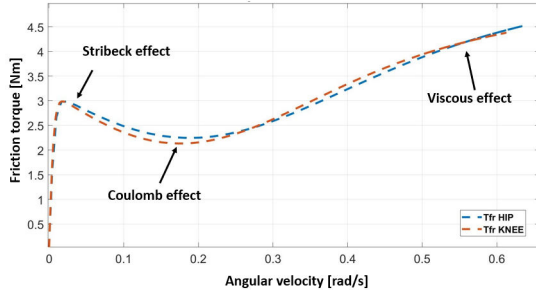


Figure 5: Hip and knee friction compensation models: the dashed blue line is the hip friction torque while the dashed red line is the knee friction torque. In the figure the different friction effects can be appreciated.

Once the models for the hip and knee joints were obtained, they were implemented within the TWIN firmware and software.

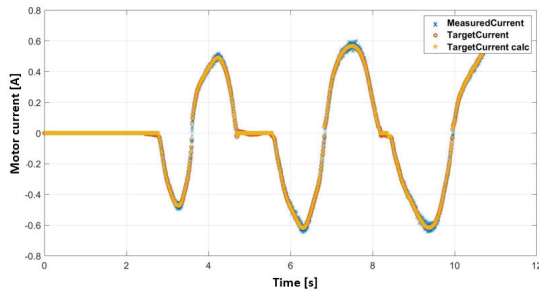


Figure 6: Motor current values comparison in the knee joint. The measured current is the blue line, the target current is the red line. As validation the yellow line is the numerical target current computed with a MATLAB simulation.

In order to get a validation that the models are working, the measured current value I_m was

compared to the target current value I , i.e. the torque control output (see equation (6)). As an example, the results for the currents in the knee joint are depicted in Figure 6. In the chart, an overlap of measured current and target current is evident ($RMSE = 0.0113A$), a proof that the torque control is working well. The yellow curve is instead the numerical target current computed with a MATLAB simulation after the test and it is overlapped with the other currents. This means that the model implemented in MATLAB has been correctly imported into the TWIN firmware. This perfect superposition, however, hides an overcompensation, which can be appreciated only in practical tests. In fact, the joint tends to be strongly unstable because the current supplied is too high. Thanks to the G parameter it is possible to regulate the contribution of compensation and make the joint more controllable.

During practical tests, even with a low friction compensation, at high speeds the joint was acquiring higher and higher accelerations and was difficult to manage, so hard that a forced stop was required for safety reasons. Investigating the problem, it was realized that the accelerations were too noisy and, even with an appropriate filtering, the instability problem recurred. So the contribution related to inertia was not included, since it is not fundamental considering the speeds and loads used in the thesis project. From the tests carried out with the new model, after neglecting inertia and setting appropriate G values (G between 0.20 and 0.60), the movement of the joint is smooth and transparent.

3.2. Impedance control

The implementation of impedance control produced the results shown in Figure 7, where the trends of electromechanical and impedance torques over angular position are described. The test to obtain this result was performed by moving the joint in one direction far from initial position and then in the opposite direction. The linear behavior of T_{des} can be noticed (red curve), whose trend follows perfectly the line with slope K . Experimentally at about 20° a torque of $1Nm$ was generated by the joint and therefore being the spring linear, the slope is $K = \frac{1Nm}{20deg} = 0.05 \frac{Nm}{deg}$. The spring effect of T_{em} (blue curve) can then be deduced. Zone 1 of the graph repre-

sents the torque when the joint is moved downwards, exactly as when a spring is pulled and moved far from the initial equilibrium point. In this case the torque tends to return with the same trend to the position θ_0 , set to 0° . Zone 2 of the graph represents instead the torque when the joint is moved upwards, like when a spring is compressed. Also in this case the torque returns to the position θ_0 with the same trend and opposite direction. The T_{em} trend has a correct torque-angle slope ($K = 0.0493 \frac{Nm}{deg}$), very similar to the torque-angle slope of T_{des} and this is an index of the correct reproduction of the desired stiffness, but a not negligible hysteresis is present, probably due to the not complete compensation of the viscous effects inside the joint.

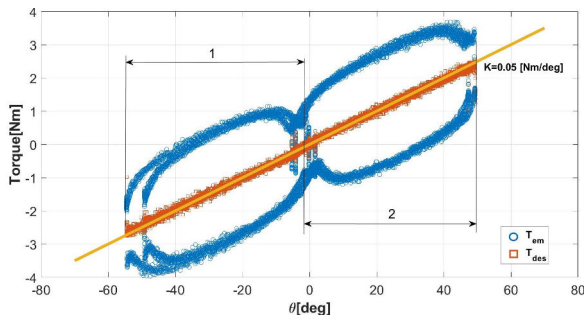


Figure 7: Trend of electromechanical torque (blue line) and impedance torque (red line) over angular position. K is the stiffness and is represented by the straight yellow line and θ_0 is set at 0°

Impedance control was validated in the same manner for the hip joint, showing the same results. While in hip-femur-knee test bench the control works properly, obviously setting a G_{knee} different from G_{hip} . In particular it is necessary to set $G_{hip} < G_{knee}$ because the geometry of the test bench changes: the weight of the femur and knee increase the torque applied to the hip and facilitate the compensation of friction.

4. Conclusion and future works

In this extended summary, we presented two models for friction compensation in hip and knee joints of the TWIN lower-limb exoskeleton. In order to generate these models, tests were performed on the joints to collect and analyze data, and then fit them appropriately. Friction compensation is performed by means of the torque controller, in which it was also possible to realize a preliminary design for an impedance control. These controls have been validated in a TWIN

single leg. The conclusions that can be drawn from this work are that in order to work in transparency, an exoskeleton needs a good compensation of friction and inertia. Despite the complexity of the friction phenomenon, this can be compensated even without the use of torque transducers, but with an adequate model. Regarding inertia instead, accelerometers are needed to transmit the angular acceleration value which is too noisy when it is computed indirectly. About the preliminary design of the impedance control, this has provided satisfactory results, making us optimistic for a future implementation that also takes into account the contribution of damping. The next step of this project, involves the realization of a finite state machine that recognizes the phase of the walk and based on the phase, sets the stiffness, the damping factor and the initial position for the hip and knee joints. We would then be able to achieve smooth impedance modulation and consequently the gait support would be patient-customized. An implementation of this nature would further increase the interaction of the human-exoskeleton system.

References

- [1] World Health Organization. Spinal Cord Injury and Stroke. URL <https://www.who.int/news-room/fact-sheets/detail>. Available online.
- [2] R. Reiner. Neurorehabilitation robotics and neuroprosthetics. *Neuroergonomics: the brain at work*, 2006.
- [3] B. Chen et al. Recent developments and challenges of lower extremity exoskeletons. *Journal of Orthopaedic Translation*, 5:26–37, 2016.
- [4] W. Meng et al. Recent development of mechanisms and control strategies for robot-assisted lower limb rehabilitation. *Mechatronics*, 31:132–145, 2015.
- [5] M. Laffranchi et al. User-centered design and development of the modular twin lower limb exoskeleton. *Frontiers in Neurorobotics*, 15:129, 2021.
- [6] N. Hogan. Impedance control: An approach to manipulation. In *1984 American control conference*, pages 304–313. IEEE, 1984.



POLITECNICO
MILANO 1863

SCUOLA DI INGEGNERIA INDUSTRIALE
E DELL'INFORMAZIONE

Analysis and compensation of friction in the TWIN lower-limb exoskeleton: a model-based approach

TESI DI LAUREA MAGISTRALE IN
BIOMEDICAL ENGINEERING - INGEGNERIA BIOMEDICA

Author: **Alessia Sacchini**

Student ID: 905539

Advisor: Prof. Elena De Momi

Co-advisors: Dr. Federico Tessari, Dr. Stefano Maludrottu, Dr. Christian Vassallo

Academic Year: 2020-21

Abstract

Exoskeletons are increasingly popular devices in the field of motor rehabilitation. However, in order to have an effective clinical benefit, patient assistance should be provided based on the level of limb impairment and the exoskeleton should accommodate the patient's efforts. Therefore, the robot has to be as transparent and compliant as possible and achieve an optimal compromise between assistance and transparency.

Transparent control is one of the biggest challenges for exoskeleton designers and there are several ways to compensate disturbances.

This thesis project aims to create a friction compensation model to increase transparency in the joints of TWIN, a lower limb exoskeleton.

After performing load tests on the joints of TWIN, which are the actuators of the entire structure, the torque contributions acting on the joints were analyzed and representative models of the friction torques were built.

The models were then used to implement a torque control within the joint. From the tests conducted employing these models and torque control, the joints appear to be transparent, with smooth and controlled motions.

In addition, this study offers a preliminary design of an impedance control, which is necessary today in rehabilitation exoskeletons, laying the groundwork for the development of an active patient assistance modality that promotes patient intentionality and improves the rehabilitation process.

Keywords: rehabilitative exoskeleton; friction compensation; transparency; impedance control.

Sommario

Gli esoscheletri sono dei device sempre più popolari nel campo della riabilitazione delle funzioni motorie. Per avere però un effettivo beneficio clinico, l'assistenza al paziente dovrebbe essere fornita sulla base del livello di compromissione dell'arto e l'esoscheletro dovrebbe assecondare gli sforzi del paziente. Il robot deve quindi essere il più trasparente e compliant possibile e deve raggiungere un compromesso ottimale tra assistenza e trasparenza.

Un controllo in trasparenza è una delle maggiori sfide per chi progetta un esoscheletro ed esistono diverse modalità di compensazione dei disturbi.

Questo progetto di tesi mira alla creazione di un modello di compensazione degli attriti per aumentare la trasparenza nei giunti di TWIN, un esoscheletro di arto inferiore.

Dopo aver eseguito dei test di carico sui giunti di TWIN, che costituiscono gli attuatori dell'intera struttura, sono stati analizzati i contributi di coppia agenti sui giunti e sono stati creati dei modelli rappresentativi delle coppie dovute agli attriti.

Questi modelli poi sono stati utilizzati per implementare all'interno del giunto un controllo in coppia. Dai test effettuati utilizzando questi modelli e il controllo in coppia, i giunti risultano trasparenti, con movimenti fluidi e controllati.

Inoltre questo studio offre un design preliminare di un controllo in impedenza, necessario al giorno d'oggi negli esoscheletri riabilitativi, ponendo le basi per lo sviluppo di una modalità di assistenza attiva del paziente che promuova quindi l'intenzionalità di quest'ultimo e migliora il percorso riabilitativo.

Parole chiave: esoscheletro riabilitativo; attriti; trasparenza; controllo in impedenza.

Contents

Abstract	i
Sommario	iii
Contents	v
Introduction	1
1 State of Art	5
1.1 Clinical context: neuro-motor rehabilitation	5
1.1.1 The role of the rehabilitative exoskeletons	6
1.1.2 Target patients	7
1.2 Lower Limb Exoskeletons overview	8
1.2.1 Commercial exoskeleton	11
1.3 Friction compensation in robotics	15
1.4 Force and impedance control	18
2 Materials and Methods	21
2.1 TWIN	21
2.1.1 Mechatronic design	23
2.1.2 Software architecture	27
2.1.3 User interface	28
2.2 Experimental setup	28
2.2.1 Test bench	28
2.2.2 Control Strategies	33
2.2.3 Testing campaign	38
2.3 Friction model	40
2.3.1 Analysis	40
2.3.2 Modeling	42

2.3.3 Compensation	44
2.4 Impedance control	46
2.5 Hip and knee joints	48
3 Results	51
3.1 Post-processing	51
3.2 Knee model	52
3.3 Hip model	53
3.4 Hip and knee models	54
3.5 Model validation	55
3.6 Impedance torque	56
4 Discussion	59
5 Conclusions	63
5.1 Future work	64
 Bibliography	 65
 A Appendix A	 69
B Appendix B	71
List of Figures	75
List of Tables	77
Acknowledgements	79

Introduction

Traumatic events or special medical conditions, can cause very severe motor impairment. Worldwide, in a large number of individuals motor function is partially or totally compromised. The World Health Organisation statistics state that every year, around the world, between 250 000 and 500 000 people suffer a spinal cord injury (SCI) and 15 million people suffer a stroke. Of these, 5 million die and another 5 million are left permanently disabled, placing a burden on family and community [1].

For these patients, neuro-motor rehabilitation is an effective therapy that helps not only to regain the ability to move, but also improves cognitive function and social, cultural, and psychological aspects of the individual. In order to achieve these results, neuro-motor rehabilitation has to include: repetitive practice of movements, task specificity, feedback on the quality of movement execution, active involvement, and variability.

In the context of neuro-motor rehabilitation, exoskeletons have great potential and play an important role. Exoskeletons are in fact wearable robots able to support (partially or totally) the weight of the body and the movement of the patient, allowing to impart forces to the user's limbs in order to generate specific movements. Thanks to the technologies integrated in their structure, exoskeletons can also measure different parameters of movement, thus allowing a quantitative evaluation of the movement and of the rehabilitation path. For these reasons, rehabilitative exoskeletons are valuable tools for clinicians to integrate with manual therapy.

However, it should be kept in mind that in order to have clinical benefit, exoskeletons should:

- adapt to the needs of the patient by varying the level of assistance according to the type and severity of the disability (at the limit, ability to work in total transparency);
- be capable of providing appropriate sensory input and feedback information to the patient;
- allow for variations in external exercise conditions and be fairly compliant with the patient's voluntary movement.

In order to meet these requirements, a proper choice of both control strategies and hardware components is essential, in a continuous trade-off between transparency, functionality and risks.

The transparency capacity of the exoskeleton in fact depends not only on the control strategy adopted, but also on the characteristics of hardware components such as weight, inertia, frictions and type of joints.

Furthermore, in the final stages of the treatment pathway, e.g., Stage V and Stage VI in Brunnstrom's classification, active patient participation is essential to shorten the rehabilitation duration and enhance training results [2, 3]. In order to obtain this level of performance, not only transparency should be increased, but the exoskeleton should provide active and adaptive assistance to promote the patient voluntary effort and intentionality.

Employing force interaction controllers is an increasingly sounded solution to achieve an active exoskeleton controller.

Goal and structure of the thesis

Based on the considerations discussed so far, the goal of this study is to compensate friction in the joints of a lower-limb exoskeleton in order to reach an adequate transparency. The exoskeleton object of this study is TWIN, developed by the Rehab Technologies Lab, of the Istituto Italiano di Tecnologia, in collaboration with the Istituto Nazionale Assicurazione Infortuni sul lavoro (INAIL).

The methodology followed to achieve this goal is a model-based approach. The reasons for this choice lie in the fact that models are powerful tools that decompose a complex system into smaller parts, easier to understand ('reductionist approach') [4]. Another interesting purpose of models is to provide a tool for measuring given quantities which otherwise wouldn't be easily derived from the real system. The power of such approach is particularly appreciated when medical devices such as exoskeletons come into play, requiring cost-effective solutions with high reliability and effectiveness.

In this thesis project a sensorless methodology to create a model for friction compensation is presented. Afterwards, with the aim of increasing the interaction between patient and exoskeleton and to align with the exoskeletons on the market that provide an active assistance, a preliminary design of an impedance controller for the TWIN lower-limb exoskeleton is proposed. This was made possible by the use of the model created.

This thesis is organized as it follows:

- **Chapter 1: State of Art.** It is explored the topic of the neuro-motor rehabilitation and how it relates with a rehabilitative exoskeleton therapy approach. Also, the main components and controls for the development of an exoskeleton are described. This chapter also provides an overview of the models and control strategies for friction compensation.
- **Chapter 2: Materials and methods.** This chapter describes the methodology followed in order to create a model of frictions acting on TWIN joints. Also the preliminary ideas to implement an impedance control are presented.
- **Chapter 3: Results.** It collects the obtained results about the new models, their validation and about the impedance control functioning.
- **Chapter 4: Discussion.** In this chapter a critical commentary about the results is provided. Also, an in-depth discussion about the main limitations of the study is developed.
- **Chapter 5: Conclusions.** Lastly, final considerations above the overall project are made, as well as suggestions about the next steps of development.

1 | State of Art

The first chapter provides a description of the main topics on which the thesis is based. In 1.1 after a brief introduction to the processes of functional recovery that occur as a result of neurological injury and that constitute the target of neuro-motor rehabilitation, the characteristics and the role that the exoskeletons must have to integrate successfully in the rehabilitation context will be discussed. This will be followed by a brief description of the characteristics of patients with spinal cord injury and stroke, identified as the main beneficiaries of the TWIN rehabilitation exoskeleton, which will help to understand their peculiarities and needs.

Subsequently in 1.2, rehabilitative exoskeletons and the principal design elements are described, with a focus on the main TWIN' competitors present on the market.

In 1.3 the physical phenomenon of friction, the models and the control strategies used for friction compensation are introduced.

The last section (1.4) presents the types of control currently used in many exoskeletons. The characteristics of these controls and their advantages will be discussed in order to understand more broadly where this thesis project wants to be placed.

1.1. Clinical context: neuro-motor rehabilitation

Neuro-motor rehabilitation is a medical practice that aims to promote recovery from neurological disorders and injuries to the nervous system. It helps the patient recover and improve cognitive function and abilities and compensate for any changes in brain function resulting from an injury or subsequent treatment.

Neuro-motor rehabilitation is commonly used to treat conditions such as stroke, cerebral palsy, Parkinson's disease, traumatic brain or spinal cord injury, multiple sclerosis, post-polio syndrome and Guillain-Barré syndrome. The purpose of this kind of rehabilitation is to promote the patient's abilities and attempt to make them as independent as possible. This involves a number of therapeutic approaches that not only aim at physical improvement, but also take into account the social, cultural and psychological aspects of the patient's personality, in order to lead to improvements in self-esteem and to help the

patient feel more confident about his or her abilities. Recovery of motor function can occur by several physiological processes [5]:

- Partial compensation of lost functions by areas of the central nervous system (CNS) unaffected by the lesion;
- Transfer of functions from the damaged brain area to healthy brain areas by generation of new synaptic connections;
- Reorganization of spinal circuits with establishment of autonomous motor patterns;
- Partial regeneration of damaged areas.

Neurorehabilitation allows to stimulate these mechanisms, applying the basic principles of motor learning [5–7]:

- Repetition: the ability to perform a movement improves with continuous and repetitive practice of that movement;
- Task-specificity: functional recovery is limited to the specific movement;
- Feedback: provides clear and accurate information about the quality of movement execution;
- Active involvement: stimulates active movement production by the patient, providing movement assistance only when required by the level of disability ("assist as needed" approach);
- Variability: includes sources of variability in the training with regard to type of exercises and external environment, leaving a certain margin of error to the patient (stimulus to the physiological process of "error correction").

The manual motor rehabilitation, although satisfying some of these requirements, has some insurmountable limits: the movement is difficult and strenuous in cases of severe motor disabilities, with consequent limitation in terms of duration and intensity of training; moreover, the movement imposed on the patient is affected by the experience and sensitivity of the therapist, and this is a disadvantage in the reproducibility of the exercises and in the objective evaluation of results.

1.1.1. The role of the rehabilitative exoskeletons

In the neuro-motor rehabilitation context it is possible to find rehabilitative exoskeletons, electromechanical devices capable of supporting (partially or totally) the weight of the body and the movement of the patient, generating and applying greater forces for longer

periods of time and following more precise and defined trajectories. They also can measure with objectivity, repeatability and precision different parameters (kinematic and dynamic ones) of movement, due to the presence of appropriate sensors in their structure. This makes possible an accurate and quantitative assessment of motor function that allows to better plan the therapeutic path (in terms of, for example, joint range and/or level of assistance provided to the movement) and to offer feedback to the patient for motivational purposes.

For these reasons, rehabilitative exoskeletons are valuable tools for the physiotherapists, allowing to intensify motor training through repetitive and task-oriented exercises and integrating with other rehabilitation techniques such as manual therapy and neurostimulation. Numerous studies have emphasized the concept of integration of exoskeletons in the rehabilitation context, contrasting it with an erroneous vision of them as rehabilitation devices for themselves and highlighting how the recovery of motor skills is optimized only if manual therapy and robot-assisted work together [6, 8].

1.1.2. Target patients

The main beneficiaries of rehabilitation with the Twin exoskeleton, the subject of this thesis, are patients affected by Spinal Cord Injury or Stroke. In this type of patients, the loss of motor function is the main source of disability and its recovery one of the main goals of neurorehabilitation [6] and of Twin of course.

Spinal Cord Injury

In patients affected by spinal cord injury, the communication between the brain and the periphery (muscles, receptors, etc.) is interrupted and causes a complete or partial loss of motor, sensory and vegetative functions related to neurons that are located below the lesion [6]: a lesion at the cervical level affects all four limbs with total or partial involvement of the trunk (tetraparesis, quadriplegia), while lower lesions affect only the lower limbs (paraparesis, paraplegia). If both motor and sensory functions are compromised, the lesion is defined as complete, otherwise incomplete.

Fortunately, motor planning and other functions related to movement generation remain intact, as brain function is not involved.

Although for incomplete lesions there is the possibility of regaining ambulatory function, in the early rehabilitation period patients are unable to maintain an upright position and walk [6]: in fact the damage to the descending pathways impairs the ability to produce voluntary limb movement, while the deprivation of the afferent pathways impairs control; in addition there are an impaired balance management, weakness of the lower limb mus-

cles, and spasticity.

Ictus

Stroke is a brain injury that can create, depending on the affected region, not only motor disabilities, but also cognitive and sensory disabilities [9]. Motor impairment originate from a deficit in the functions of motor gesture planning and/or form a deficit in the nerve impulse generation [5].

One of the major limitations of stroke patients is the degradation of walking pattern. The typical factors that cause deterioration of walking abilities are [2, 6]: hemiplegia or hemiparesis of the lower limbs (so respectively complete or partial loss of motility), spasticity (abnormal increase in muscle tone, often resulting in involuntary spasms), muscle weakness, unusual muscle synergies (loss of control of some muscles and consequently involvement of other muscle groups to perform the movement), altered timing of muscle activation, proprioceptive disturbances in the ankle.

The result is a slow, asymmetrical, and metabolically inefficient gait [6, 9]. Therefore the patient has difficulties in managing the bilateral synergies proper of the locomotor pattern, in maintaining balance and progression on the plegic limb, in positioning well the foot on the ground, and in adapting the gait in response to changes in the external environment.

1.2. Lower Limb Exoskeletons overview

The term exoskeleton comes from the Greek words “exo” = outer and “skeletos” = skeleton, so it is an external structure that supports and protects the body. Powered exoskeletons are wearable robots attached to the human limbs, which replace or enhance their movements [10].

As the word itself suggests, since these devices are skeletons, they consist of links and joints that replace human joints.

The joints in the lower limb of the human body are the hips, knees, and ankles. Each joint has different movements or degrees of freedom (DoF): the hip has 3 DoF (flexion-extension, abduction-adduction, internal-external rotation), the knee has 2 DoF (flexion-extension, rotation) and the ankle has 3 DoF (plantar flexion-dorsiflexion, abduction-adduction, eversion-inversion). The types of lower limb exoskeletons based on joint motions are differentiated into several types based on how the actuators drive the exoskeleton. In fact the actuators can drive just hips, the knees, the ankles or a combination of joints, depending on the target patients. These combinations of actuators are hips and knees, as

in Twin for example, knees and ankles, and all three joints [11].

In the design of an exoskeleton, the key elements are actuators, sensors, power supplies, control strategies, and materials. In this overview, the main strategies that have been adopted are described.

Actuators

Depending on the source of motion the actuators can be distinguished in active actuators or passive ones. An active exoskeleton is one that uses a power source to activate the actuators. Therefore it can be electric, pneumatic, or hydraulic. On the other hand, a passive exoskeleton is a device that has no power source. So this type of exoskeleton use for example springs and dampers [11].

One of the main issues is to make actuators lighter and more performing. Size, weight and power efficiency of motors have historically limited robotic exoskeletons. To provide the physiological torques required, a significant amount of weight, inertia and size needs to be introduced to the exoskeleton to include actuators, batteries and controllers. Nowadays the main choice about actuators is electronic motors, while the hydraulic and pneumatic ones are less common. This choice is done for multiple reasons: servo motors are capable of very advanced position-based control that is much more difficult to achieve with pneumatic and hydraulic systems and especially, for the exoskeletons that work with spinal cord injury and other disable individuals, electrical motors allow different kind of position control and can coordinate multiple degrees of freedom. Brushless DC motors are popular in exoskeletons due to their high torque to weight ratio, reduced noise and reliability. Because of fast accelerations of human legs during locomotion, gear ratios cannot be made too large, which limits the torque assistance of electric actuators.

Sensors

Sensors are necessary devices for controlling robotic exoskeletons. Every exoskeleton has at least some form of mechanical sensor to help regulate position, force or torque. Most exoskeletons encode joint position which helps to regulate safety and provides a phase variable to modulate torque output. In addition, many lower limb exoskeletons use a position controller and try to specify a precise joint angle trajectory that the exoskeleton cycles at each step phase. Many, but not all, exoskeletons use force sensors. Commonly, they involve force sensors in the feet which measure ground contact force. This approach helps by providing different control states for stance and swing configurations and can be sometimes used for more complex control measurements and control such as center of pressure. Accelerometers and gyroscopes are occasionally included. Obviously at the ex-

perimental level, for the purpose of improving control and human-machine feeling, brain, neural or muscle signals can also be used, but in commercial exoskeletons, which are the ones presented here, these solutions are not yet implemented.

Power Supply

Also power supply is a constraint in the design of wearable exoskeletons. More energy requires more weight which tends to decrease the overall functionality of the device. Almost all the exoskeletons use batteries to generate the necessary energy for a powered system. The most common solution is to use lithium ion batteries. In fact they provide 1-5 hours of functioning and help to reduce size and weight increasing power density. Many clever designs have included mechanical elements such as springs and clutches to store and release energy similar to biological tendons. These designs along with improved batteries can enable portable exoskeletons to function over a significant period of time[9].

Control

With respect to the elements described above, control strategies for the exoskeleton tend to vary widely from design to design in existing prototypes and commercial products. The patient and exoskeleton interact from the control aspect and form a kind of cooperative system, as shown in Figure 1.1.

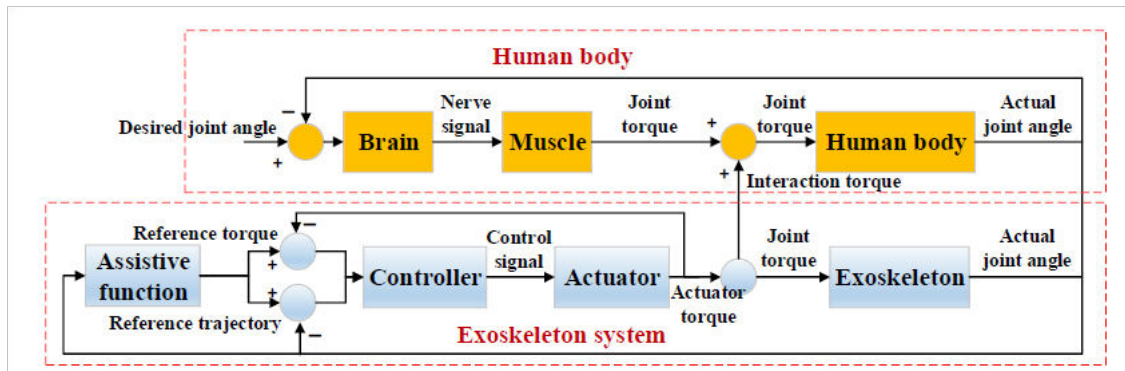


Figure 1.1: Schematic of the human-exoskeleton cooperation system [12].

As for the exoskeleton system, the reference torque/trajectory is obtained based on the assistive function and enters the controller. A control signal is then produced that drives the actuator, and the actuator produces a torque. The joint torque is used to drive both the patient and the exoskeleton. In this human-exoskeleton system, the human body involvement can be different. In the case of rehabilitative exoskeletons, the joint torque expressed by the patient is small due to muscular impairment (even zero in the case of paralyzed patients), so the exoskeleton through the interaction torque predominantly as-

sists the patient [12]. The control strategies of exoskeletons in gait rehabilitation can be generally divided into two main categories: trajectory tracking and assist as needed (AAN). Regarding the first one, under a predefined gait trajectory control mechanism, the desired joint trajectory is pre-recorded from a healthy person, or extrapolated from a gait analysis data, and then replayed on an exoskeleton [12]. This implies that motor function of the limb is promoted and muscle atrophy is reduced, but the patient is assisted passively, and thus there is a lack of patient motivation and initiative. This control is useful when the user has a low ability to interact with the system or control the exoskeleton [13]. However, it limits too much in the case of rehabilitation, where interaction is necessary. By contrast, with an AAN control strategy, the device contribution to movement is based on the patient's effort and physical condition. This solution promotes patients intention, motivation, encouraging them to trigger the exoskeleton assistance by their own active effort [12, 13]. Hybrid position/force controls and impedance controls belong to this category. A more in-depth discussion of how these controls work can be found in 1.4. A more responsive controller is a proportionally applied force based on a specific sensor such as an EMG measurement from a relevant muscle or a force sensor between the user and the exoskeleton. These are adaptable to different situations, but are complex to implement in a real-world device[13]. They are still in the research phase. There is no general convergence of solutions for exoskeleton control, and most of the controls used are not explicitly presented. In fact the exact control algorithms for many exoskeletal devices are not well documented in literature, especially for commercial ones.

Material

Another important property of exoskeletons is the frame design, which can greatly influence the overall performance of a robotic exoskeleton. Most exoskeletons have a rigid metal structure. Some type of aluminum alloy is used to create the connections between the joints, this choice is made to make the structure as light as possible, yet rigid and able to support the patient and physiological forces. Titanium is the best material in terms of strength and weight, but it is considerably expensive. An alternative material that is sometimes used is fiber-reinforced plastic, such as carbon fiber.

Overall, rigid metal structures of aluminum, titanium, or steel are the common design material for any exoskeleton that implements multiple degrees of freedom.

1.2.1. Commercial exoskeleton

In this paragraph the focus is on commercially available devices, i.e. Twin's major competitors, which are described in order to have a clearer view of the market in which TWIN

will operate, but also to understand their strengths, weaknesses and opportunities.

Indego

Indego, manufactured by Parker Hannifin, is a wearable exoskeleton that actively assists people to stand up and walk. It consists of five interconnected components: the pelvis and the upper and lower sections of the left and right leg. The pelvis component houses a rechargeable battery, a central processor, and a Bluetooth module, while each leg component contains two motors and integrated sensors that provide information about the user's posture and inclination. Using this data, the exoskeleton can be controlled through postural modifications. There are LED lights on the pelvis unit and vibration feedback to inform both the therapist and patient of the machine's status and mode of operation. While functioning the exoskeleton, the use of crutches is mandatory to improve stability. Users can walk on even or uneven ground up to approximately 5° and perform transitions from sitting to standing and standing to sitting [14].



Figure 1.2: Indego exoskeleton by Parker Hannifin.

Ekso

Initially called eLEGS, Ekso is a lower extremity exoskeleton made by Ekso Bionics. It was created for use as a walking training device by individuals with motor impairment. The FDA has approved its clinical use for post-stroke or SCI patients. Ekso is composed

of metal segments, easily worn by the patient, laced to the body by straps to support the legs, feet and torso. The movement is made possible by motors placed on the hip and knee joints, powered by a battery placed on the torso support, while ankle is passively actuated with a spring. The exoskeleton is equipped with a graphical interface that allows you to specify the parameters of the walk and start the steps in a controlled (by the therapist) or autonomous way. Choosing the latter mode, to start the step it is necessary to make a weight shift forward. The main feature is the possibility of varying the degree of assistance provided according to the patient's needs and residual abilities. It cannot be used without a cane, crutches or a walker and cannot be used by the patient to climb or descend stairs. used by the patient to climb or descend stairs [15].



Figure 1.3: Ekso exoskeleton by Ekso Bionics.

ReWalk

ReWalk is a wearable robotic exoskeleton, made by ARGO Medical Technologies, that enables people with spinal cord injury (SCI) to stand, walk, climb and descend stairs. Movement is made possible by motors located on the hip and knee. Control of the device is made possible by a remote controller (wireless communicator) controlled by the user, a tilt sensor and specific body movements. The remote controller allows the user to select

the mode of operation: Sit-To-Stand; Walk; Stand; Stand-To-Sit. A visual indication provides information on the status of the system. If the selected mode is Sit-To-Stand, the user, while seated, has to wait three seconds for the exoskeleton to help him or her stand up. The Walk mode, on the other hand, allows the user to control the exoskeleton and therefore the walk through postural movements. Specifically, if the inclination of the trunk in the sagittal plane overcomes a predetermined threshold, the exoskeleton starts walking. The Stand mode allows the user to stand still in an upright position and is used so that the user, even if they fall into error by exceeding the flexion threshold for walking, cannot trigger the step. The last mode, Stand-To-Sit, is used to make the exoskeleton sit, the user has to wait three seconds after the selection for the exoskeleton to start this phase. The sensor for evaluating the trunk angle is located on the pelvic belt. In addition to the exoskeleton, the patient must wear a backpack where the components of the power management system and computer control system are housed. The main battery is a lithium-ion battery capable of allowing continuous walking for more than two hours. Crutches are required during use of the ReWalk in order to provide stable support during both standing and walking. Installation of the exoskeleton, customized for each patient, is performed by an ARGO-trained health care professional. The following lengths can be adjusted: from the knee joint to the ankle (tibia), from the middle of the hip to the middle of the knee (femur) and the pelvic belt. Adjustments can also be made for variables associated with the patient's gait such as: knee and hip flexion-extension, maximum speed, trunk angle, and pause time (time between steps). The values of these parameters are adjusted according to user preference, ability and experience level. The device has safety and emergency hardware and software features that stop the activity. Both software limits and mechanical stops are present so as to prevent excessive joint flexion-extension. Finally, in the case of a major system failure, such as complete loss of power the ReWalk will run a "graceful collapse" algorithm that gently lowers the user to the floor [16].



Figure 1.4: ReWalk exoskeleton by ARGO Medical Technologies

1.3. Friction compensation in robotics

Every time precise motion control of a robotic system must be achieved, friction compensation presents a challenge to the designer, who must solve various theoretical and practical problems.

Friction in fact is a complex phenomenon that occurs when there is relative motion between two surfaces in contact, as a consequence of the irregularities and asperities at microscopical level, and depends on many factors such as the geometry and materials of the two surfaces, their relative velocity, the presence of lubricants, temperature, and so on [17].

The effects of friction are particularly critical for robots: it has been observed [18] that "friction can cause 50% of the error in some heavy industrial manipulators." Poor friction compensation can lead to significant tracking errors (especially at low speeds), stick-slip movements, and limit cycles when speed reversals occur in the assigned trajectory. Then, in the case of rehabilitative exoskeletons, where precise motion control is necessary to properly perform therapy and not further impair the patient's movements, compensating friction becomes critical.

Different friction models and control solutions can be found in the literature, thanks to

the experimental observation of friction phenomena, but no strategy can be considered more effective than others, since the phenomenon is complex. The choice of a particular friction compensation technique must be made taking into account the characteristics of the robotic systems considered and its hardware/software control architecture, sensor accuracy, actuator characteristics and real-time constraints [19].

Friction models

Generally, models can be divided into two categories: static models and dynamic models. In the first kind, the friction force is a static function of velocity. An example is the Coulomb model, in which the frictional force is assumed to be independent of velocity. Also viscous friction is added in which the force is proportional to velocity:

$$F(v) = F_c \operatorname{sgn}(v) + \beta v \quad (1.1)$$

where F is the frictional force, v is the relative velocity, F_c is the Coulomb friction, and β is the coefficient of viscous friction. Thanks to experimental observations, it is known that the transition from stiction to friction during motion is not discontinuous, and in order to account for this continuity in the transition, several mathematical models have been formulated. These take into account the Stribeck effect, i.e. the decrease of friction as velocity increases within the Stribeck region at low velocity. Model (1.1) then becomes:

$$F(v) = [F_c + (F_s - F_c)e^{-|\frac{v}{v_s}|^{\delta_s}}] \operatorname{sgn}(v) + \beta v \quad (1.2)$$

where v_s is the Stribeck velocity defining the region where this effect is present, and δ_s can be equal to 2 (but not necessarily). This is the simplest static model that can be implemented and an effective alternative is to use a polynomial expression or sigmoid-functions to better account for the complexity of the phenomenon [19].

Dynamic models, on the other hand, take into account non-stationary velocities, small displacements that occur during stiction, and possible hysteresis effects. Examples of these model types are the Dahl model, the generalized Maxwell-slip model, and the LuGre model [17].

Strategies for friction compensation

In addition to the models described so far, various strategies can be adopted to eliminate or reduce the effects of friction on the robot motion. It is possible to classify the control strategies in the following way [19]:

1. A "fixed" friction compensation term is added to a more general control scheme. Friction parameters are estimated off-line, based on the chosen model (the more complicated and accurate the model, the higher the number of parameters to be estimated) and following appropriate identification procedures. An additional correction can be added to the a priori estimated compensation term. If a dynamic friction model is considered, an observer is inserted to estimate the internal state of friction.
2. Only certain characteristics of friction phenomena are considered for compensation. Also in this case, a compensation term that accounts for friction is added to the control scheme, but without requiring the knowledge of the exact friction model.
3. On-line friction compensation by model-based adaptive algorithms. The parameters are tuned on-line and thus satisfactory compensation can be achieved even with high variations. These strategies often require significant on-line computational load, and high precision sensors especially if dynamic friction models are also used.
4. Compensation is accomplished by some strategies that are not based on a specific model, so it is necessary to correctly choose control gain parameters or using non-model-based observers. In these strategies, the effects of friction are estimated and compensated with other disturbances that affect the motion of the robot.
5. Friction compensation with soft computing approach, using fuzzy, neural and genetic algorithms to reconstruct the friction torques or for the self-tuning of controller gains.

The solution 1) is the "cheapest" to implement since the on-line computational cost required is limited, but an accurate friction identification phase with a good off-line estimate of the friction parameters (possibly with high precision sensors) is required. For example, a compensation term based on the pure Coulomb + viscous friction model (1.1) cannot provide accurate tracking and positioning results, while adding the Stribeck effect term, the results are better. However, these strategies do not account for friction variations (for example variations with time or temperature). In order to account for these variations, an adaptive compensation approach is more appropriate. An alternative may be to use strategies such as 1) and 3) together: a model is identified and parameters are estimated off-line, then corrections are made on-line [19].

1.4. Force and impedance control

The patient's rehabilitation process is developed in three different stages, namely preliminary, intermediate and advanced stages [13]. During these stages, the patient gradually regains muscular strength and the ability to move, so in parallel, the assistance provided by the exoskeleton to the patient also varies gradually and provide compliant motion.

During the preliminary stage, passive control is required to allow the compromised limb to achieve continuous and repetitive training. For this stage, *position control* is favored, where a specific trajectory is recorded from healthy subjects and then replicated by the device. However the movement is less compliant, it is not customized on the patient, but above all this control reduces the active interaction with the wearer.

After a period of training, if the patient has regained muscle strength, the robot should provide active and adaptive assistance in order to promote the patient's intention and initiative [13]. A very effective solution to get a compliant active exoskeleton controller, is to use force interaction controllers, mostly used in form of either the *impedance or admittance controllers* [20]. These controllers in fact are able to reduce or possibly zero the interaction force of the human-exoskeleton system.

The basic concept of the impedance controller is: it accepts position and produces force. While, the admittance is the opposite of the impedance controller, so it accepts the force and yields the position.

Nowadays, more and more exoskeletons control the interaction forces by using impedance control algorithms [13].

Impedance control

The concept of impedance control in the field of robotics has been introduced by Hogan [21]. The power flow between two physical systems can always be defined as the product of two conjugate quantities: a (generalized) effort and a (generalized) flow. In the electrical context, the flow is the current while the effort is the voltage. In the mechanical context, however, the flow is the velocity (linear or angular), the effort is the force (or torque) [21].

Mechanical impedance is therefore defined as a dynamic relationship between force and velocity (or displacement) for a mechanical system.

Impedance control aims in particular to ensure that the manipulator (the joint in the case of the exoskeleton), controlled in position and in interaction with the environment, manifests the behavior of an impedance, assimilated to a generalized mass-spring-damper system [22]. A model of a second-order mechanical system with interaction force is shown in the Figure 1.5.

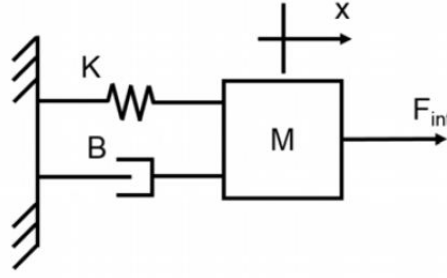


Figure 1.5: Mass-spring-damper system: K is the spring stiffness, B is the dumping and F_{int} is the interaction force

Spring: each impedance has a stiffness as the lowest order term, i.e., a static relationship between the output force and the displacement. Defining x_0 the desired equilibrium position of the end effector in the absence of external forces, and $x = L(\theta)$ the position of the end point, derived by direct kinematics from the information about the joints, the following formulation is obtained [21]:

$$F = k \cdot (x_0 - x) \quad (1.3)$$

where k is the elastic stiffness and F is the elastic force resulting from the position error $x_0 - x$.

Damper: as a first-degree term the impedance has a damping, which is a relationship between force and velocity, as shown in the expression below [21].

$$F = B \cdot v \quad (1.4)$$

where B is the damping.

Combining then the contributions:

$$M\ddot{x}(t) + B\dot{x}(t) + Kx(t) = F(t) \quad (1.5)$$

which in the Laplace domain is written as:

$$X(s) \cdot (Ms^2 + Bs + K) = F(s) \quad (1.6)$$

Then the transfer function, displacement input - force output, called *impedance* is [22]:

$$Z(s) = \frac{F(s)}{X(s)} = Ms^2 + Bs + K \quad (1.7)$$

In the time domain, the impedance can be expressed by the differential equation:

$$M(\ddot{x} - \ddot{x}_d) + B(\dot{x} - \dot{x}_d) + K(x - x_d) = F_x \quad (1.8)$$

where x is the actual position, x_d is the desired position and M , D , K , and F_x are the inertia, damping, stiffness, and force matrix, respectively [21].

By varying the impedance, the interaction varies, in particular, in the case of rehabilitative exoskeletons, increasing the impedance, increases the assistance to the patient to lead the limb along the reference trajectory, on the contrary a low impedance implies that the patient needs less assistance [12].

2 | Materials and Methods

This second chapter describes the materials and methods used in the thesis project, which led to the friction compensation model and subsequently to the implementation of impedance control.

After a description of the TWIN exoskeleton in 2.1, the experimental setup and the test campaign performed are presented in 2.2.

Section 2.3 shows how the friction compensation model was created and then implemented on the TWIN joints.

This chapter concludes with the impedance control development (see Section 2.4) and with the application of the methods to hip and knee joints (see Section 2.5).

2.1. TWIN

TWIN is a powered exoskeleton developed by the Rehab Technologies Lab, of the Italian Institute of Technology, in collaboration with the National Institute for Insurance against Accidents at Work (INAIL). TWIN is designed for people with spinal cord injury or stroke [23].

The exoskeleton is ideal in areas reserved for rehabilitation therapy and should only be used on compact, dry, flat surfaces. Furthermore, during its use, the use of a walking aid, such as crutches or a walker, is mandatory (see Figure 2.1c). Its structure provides the control of the knee and hip joints by means of four motors and five rigid sections: a pelvis and two separate components, for each leg, of the femur and tibia.



(a) TWIN exoskeleton.

(b) Assembling TWIN.



(c) TWIN exoskeleton worn by a patient.

Figure 2.1: TWIN structure and wearability. In the figure (a) the details of the TWIN structure can be appreciated. The figure (b) shows a patient wearing the different TWIN components without any external help. In the figure (c) the patient is standing and able to walk with crutches.

The distinctive feature of this exoskeleton is its complete modularity: the exoskeleton can be disassembled by the user into small sub-units without the need of additional tools, so as to facilitate its management, donning and transportation, as shown in Figure 2.1b. This is possible through a quick-disconnect (QD) system that realizes both mechanical and electrical connections [24].

It is possible to use Twin in different modes: Sit-Up, Sit-Down, Walk Mode, Gravity, TwinCare. Within the Walk Mode it is also possible to choose between two execution modes: Manual Mode and Automatic Mode. In Manual Mode, each step is manually triggered by the therapist through the mobile device associated with the exoskeleton (a tablet). In Automatic Mode, the patient can intentionally start the walk with postural movements by overcoming and maintaining a predetermined threshold of trunk flexion. In both cases the trajectory is predetermined.

The Gravity walking mode is designed to allow the use of the exoskeleton for patients who have some residual autonomous mobility in the limbs, leaving the patient free in the setting of the walk and helping him to not feel the weight of the exoskeleton that he wears, thanks to a gravity compensation.

The TwinCare gait mode allows the exoskeleton to be used by patients with residual independent mobility with different degrees of motor impairment. The user can choose the degree of assistance, meaning that the exoskeleton can adapt to patients who require differentiated support between the two limbs and/or between the various joints. This is possible thanks to a friction compensation.

2.1.1. Mechatronic design

TWIN's specifications are shown in Table 2.1. These values are based on the anthropometry of the European population, on the engineering constraints and on the comparison with other exoskeletons.

Type	Value
Target walking speed	1.5 km/h
Max patient's weight	110 kg
Target weight	20 kg
Battery autonomy	4h
Min-max sizes	5 th to 95 th percentile

Table 2.1: TWIN's specifications [24].

Actuators

Hips and knees are actuated by a Maxon EC90 flat motor, coupled to a 100:1 CSD Harmonic Drive gear. The motors employed for the knee and hip have different nominal voltages, 24V and 36V, respectively, to meet the different torque/speed requirements of these two joints.

Structural parts

The structure of the TWIN exoskeleton is largely made by welded Al7075 T6 aluminum alloy profiles, which has low weight and minimize cost [24]. The Figure 2.2 shows all the elements of the structure.

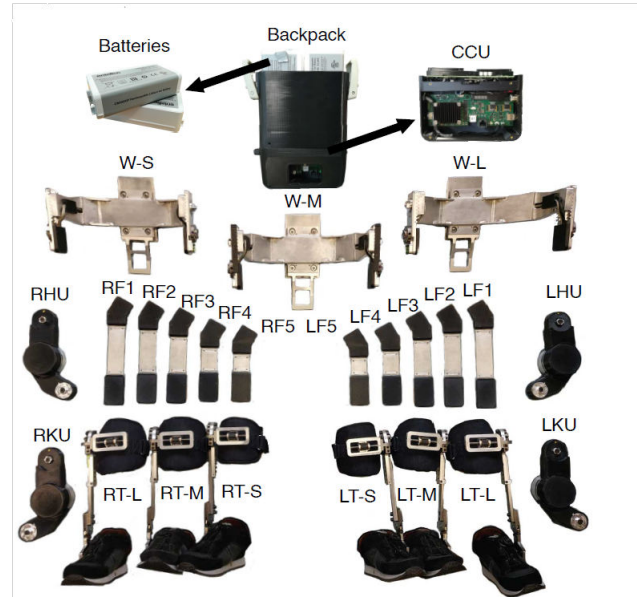


Figure 2.2: Structural parts of TWIN: from the top, batteries, backpack, Central Control Unit (CCU); W-S/M/L are 3 waists sizes; RHU and LHU are right and left hip motor unit; RF1-5 and LF1-5 are the different femur sizes; RKU and LKU are right and left knee motor unit; RT-L/M/S and LT-L/M/S are right and left tibia sizes [24]

In the backpack there are the batteries and the central control unit (CCU) that can be easily changed. The backpack is connected to the waist module that are available in three sizes in order to cover the set anthropometry requirements.

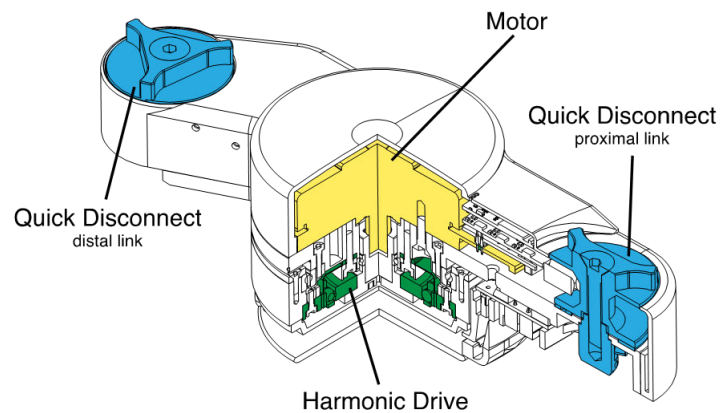
The femur modules are composed of a straight link that ends on both sides with receptacles of the quick disconnect system. Six sizes are available in order to satisfy different physicality. While the tibia comes in one size because is provided with a regulation system that can assume different lengths. The upper part of the tibia has the receptacle for quick disconnect system, while the lower part is connected to the foot through a ankle-foot

orthosis (AFO) [24].

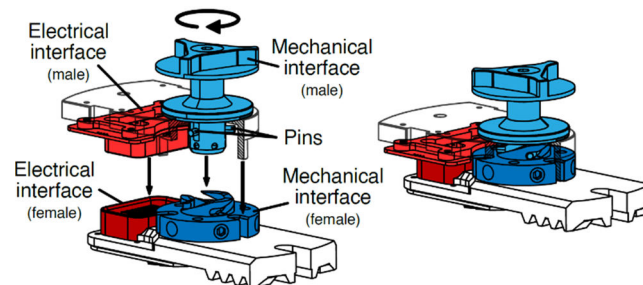
Joints

Joints are the most characterizing components because are responsible for housing the actuators. In particular the quick disconnect was a critical element to realize since it must achieve high stiffness and safety. The QD is made of a mechanical interface and an electrical interface (see Figure 2.3).

As Laffranchi describes, "the mechanical interface uses a male part with three pins placed radially which engage into a female part grooved in a way such that clockwise rotations of approximately 120° will result into insertion of the male part into the female part. The user can connect or disconnect the joint moving the a handle on the male part. Safety plungers located radially into the female part engage into holes manufactured onto the male part to give feedback to the user when the connection is complete and to resist to accidental openings. The electrical interface is made with standard electrical "board to board" connectors that are used to deliver both voltage supply and the CAN communication to the motors" [24].



(a) Actuation module.



(b) Quick disconnect system.

Figure 2.3: Internal structure of a TWIN joint: the electrical interfaces are in red, while the mechanical interfaces are in blu [24].

Braces

Braces are the interfaces between the patient and the machine (see Figure 2.4). Their inner part in contact with the patient is made of spandex, which ensure biocompatibility and reduces shear forces on patient skin, while the external part is made of using jeans fabric for durability. In order to facilitate the donning procedure and the correct positioning, all braces employ Velcro straps [24].



Figure 2.4: Waist, femur and tibial braces and their DOF's [24].

The waist brace is composed of a central portion which is directly connected to the structure by means of bolts and two lateral bands wrapped around the patient and can be tightened on the front. This brace houses a coccyx support which avoids excessive lumbar hyper-lordotic posture. A semirigid shell, which can tilt in the transversal and sagittal plane, is placed on top of the coccyx support inside the brace to allow rotations of the sacrococcygeal region to avoid generation of shear stress on the patient's skin (see Fig 2.4 – top right). The frontal portion of the brace acts as a thoracic stabilizer preventing the patient from collapsing, which is critical for patients with higher level of injury. Each thigh can partially rotate (see Fig 2.4 – middle right) around the femur, which ease donning/doffing procedures and speed up size replacement. The shank brace is composed of a hinged semirigid plate which hosts the patient tibia and can tilt in the sagittal plane. The medio-lateral position of the brace can be adjusted to account for different postures or deformities in the knee joint by means of a leadscrew mechanism (see Fig 2.4 – bottom right) [24].

2.1.2. Software architecture

The software structure of the Twin exoskeleton is a six point star client/server structure: four motors, a battery and one Inertial Measurement Unit (IMU). The central control unit (CCU) is a custom board implementing a Zynq SoC, based on an ARM Cortex A9 processor which has to monitor the battery pack and the 6-axis IMU sensor. The file system of the CCU was built with the help of the Buildroot tool, in order to create a lightweight Linux Ubuntu environment. Each motor is controlled and actuated locally by a logic board based on the TM4C1294NCPDT: a 32-bit ARM Cortex-M4F microcontroller provided by Texas Instruments that communicates with the CCU via a CAN port at a frequency of 500Hz using socketCAN residing in Linux. Similarly, the battery is connected to CCU and constantly controlled via its I2C interface. Within this structure, the CCU performs high-level control of the exoskeleton and enables the movement of the articular joints by receiving and sending commands and measurements to/from each motor. During the walking activity, each execution of the of the step, the CCU generates and sends a new set of the positions to be reached to the motors. The trajectories are subsequently managed at the joint level by a position control based on a proportional-integrative (PI) controller operating at a frequency of 20 kHz [23]. The logic structure of TWIN is shown in Figure 2.5.

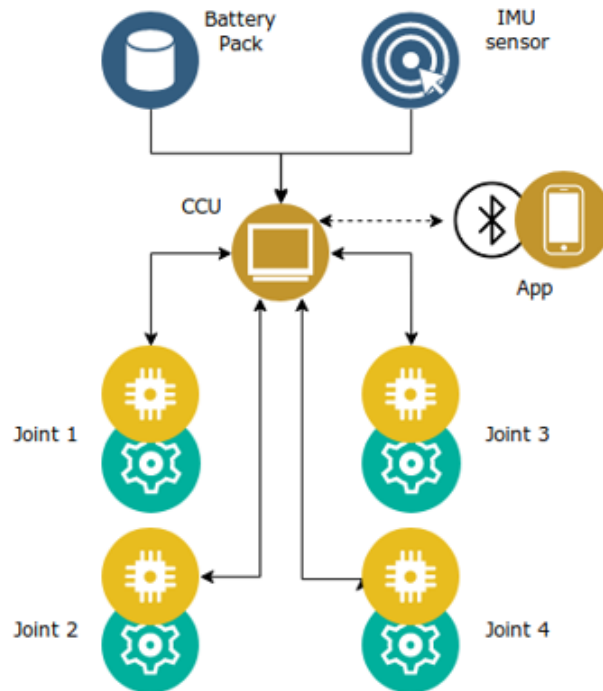


Figure 2.5: Logic structure of TWIN. The main elements of the control software are in yellow, the green parts are the actuators [23].

2.1.3. User interface

The exoskeleton is operable using a Bluetooth communication made possible by any Android device through an app . This app allows the user and the clinicians to perform all the movements and to configure all the parameters that are necessary to create a personalized therapy. Each session, for each user, is saved in a database on the exoskeleton that can be extracted for clinical purpose. The user can activate and deactivate the different modalities according to the patient's needs by interacting with the app. Moreover the app returns in real time all the main information about the status of the device and the battery status, accounting for the patient's safety.

2.2. Experimental setup

2.2.1. Test bench

This thesis project aims first of all to carry out a friction analysis of TWIN, therefore the exoskeleton is separated into its fundamental parts: the joints. The idea is to start from a TWIN joint and see which losses act on the joint and then quantify them. To do this, an ad hoc test bench was built, as shown in Figure 2.6.

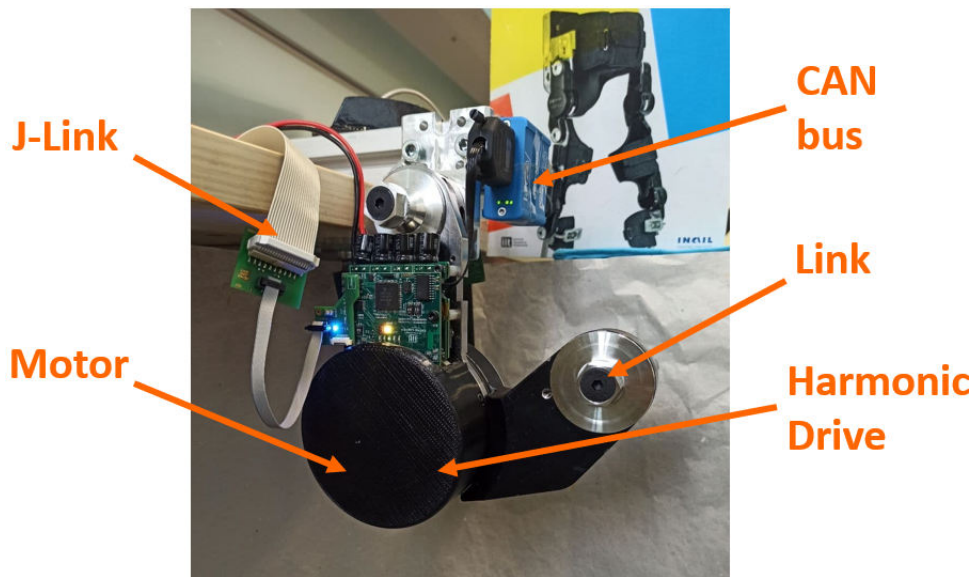


Figure 2.6: TWIN's joint and the main elements of the test bench: the motor and the harmonic drive are inside the black cover, the J-link and the CAN bus are connected to the PC. In this figure the quick disconnect system is clearly visible at the extremity of the rigid link.

The joint was secured to the table with a bracket equipped with the housing for the quick disconnect and the bracket in turn was secured to the table by means of a bench vise. The joint test bench can be schematized with a diagram that shows its fundamental elements:



Figure 2.7: Schematic diagram of the joint test bench

A detailed description of the various elements is offered here.

Power supply

The CMX820P (see Figure 2.8a) is a high power 28.8V 3.2Ah Lithium Ion Smart battery with a stored energy of 92.2Wh. It is designed to meet the demanding needs of medical device manufacturers. The latest Nickel-Manganese-Cobalt Lithium ion cell technology within the CMX820P allows it to discharge continuously at up to 15A (or 330W continuous) making it ideal for high power transportable devices - either as a primary power source or as a redundant backup supply. A clear 5-bar LCD display on the rear of the battery provides a quick visual capacity reference for the user so they can decide when to charge it [25].

Inverter

Each electric motor construction technology requires a particular type of "driving" and this is the task of the inverter or driver. The input interface to a motor driver has the task of communicating the desired functionality to the motor, respecting the limits of the circuit capacity and kinematics. The logic inside the driver processes the user's request by providing output signals suitable to drive the generic amplification stage. The amplification stage, in turn, mixes the input electrical quantities from the power supply: voltage, frequency, current, etc.. and transforms them appropriately to drive the electric motor connected to its output. The motor could, if necessary and if supported by the driver, provide feedback signals to the driver through appropriate sensors, for example limit switch, encoder or Hall-effect sensor.

In this case a DRV8301 Three-Phase Gate Driver (six-step) from Texas Instruments is used [26].

Motor

Actuation is performed by a DC motor that converts electrical energy into torque. DC motors are very used in the biomedical field where efficient speed and position accuracy is required, moreover their sizes are small.

DC motors can be divided between Brushed and Brushless motors. The main difference between the two, as one can easily deduct from the names, is that Brushed motors presents brushes meanwhile the Brushless don't.

BLDC motors are a type of synchronous motor because the magnetic fields of the stator and of the rotor rotate at the same frequency. There are different configurations, but the most popular and widely used is the 3-phase BLDC motor, so the stator has 3 windings. As compared to brushed DC motors, the BLDC ones are electronically commutated: the stator windings are energized in sequence and the motor rotates. In order to understand which winding will be energized, it is important to know the rotor position. This is in fact sensed through Hall sensors embedded into the stator. Moreover, most of the motors are equipped with an optical encoder which gives two signals with 90 degrees phase difference; using these signals, both speed and direction of rotation can be determined.

Also, most of the encoders give a third index signal, which is one pulse per revolution. This can be used for positioning applications where the dynamic responses of speed and torque are important[27]. These applications in fact may have frequent reversal of rotation direction and a varying load and this is the case of an anatomical joint, for example. Under these circumstances having an encoder that measures true speed and relative position is important.

BLDC motors have many advantages over brushed DC motors and induction motors. A few of these are:

- Better speed versus torque characteristics
- High dynamic response
- High efficiency
- Long operating life
- Noiseless operation
- Higher speed ranges

In addition, the ratio of torque delivered to the motor size is higher, making it useful in applications where space and weight are critical factors, like in the case of an exoskeleton. After all these considerations, it is safe to say that a BLDC motor is the most appropriate motor for a knee or hip joint. In fact the motor used in the test bench is an EC90 flat, brushless, with Hall sensors from Maxon. His rated voltage is 24V, so it represents the

joint of a left knee. Also an encoder is present in order to perform the position control (see Figure 2.8b) [28].

Microcontroller

The motor is actuated by a logic board based on an ARM Cortex M4 microcontroller unit. The test bench uses a TM4C1294NCPDT microcontroller from Texas Instrument's Tiva™ C Series [29].

Gearbox

A fundamental element is the transmission unit, which regulates the speed and the torque of both motor and loads, thus allowing the transition from high speed and low torque to low speed with high torque. It is characterized by the transmission ratio τ , which in our case is equal to 1:100. In the joint the Harmonic Drive (HD), model CSD-25-100-2A-GR-BB, is used (see Figure 2.8c). It is a particular gear belonging to the family of harmonic gears [30]. This type of gear is often used for several reasons:

- Zero backlash;
- Excellent positioning accuracy and repeatability;
- Small size and minimal weight;
- High reduction ratio in a single stage;
- Central through hollow shaft (through this central hole, cables, power supplies, laser beams and so on can easily pass);
- High reliability and long service life.



(a) Battery



(b) Motor



(c) Gearbox

Figure 2.8: Some elements of the test bench: the figure (a) is the Lithium Ion Smart battery, figure (b) is the Maxon EC90, while the figure (c) is the Harmonic Drive.

The joint was then connected to the PC, a Dell XPS 15, and the communication between the two was via a JTAG cable and CAN bus. These elements are discussed in more detail below. From the PC, through the user graphic interface, it is possible to select the type of joint and therefore the motor used, but also the kind of controller to activate. After the joint has been moved for some tests and once the control is disabled, it is possible to measure position, current, voltage bus, velocity and duty.

JTAG emulator

JTAG emulators are the "umbilical cord" between PC software tools and DSP boards during development. Typically connecting to the host PC via parallel port or USB port, the JTAG emulator provides a standard, simple way to give the development tool software a direct connection to one or more DSP devices on the target board. In the test bench a J-Link EDU from Segger is used (see Figure 2.9a). The USB cable allows the connection with the PC, while the ribbon cable connects from the target to the microcontroller [31]. Thanks to this element the firmware can be uploaded onto the joint logic board.

CAN bus

The Controller Area Network (CAN) is a serial communication protocol capable to efficiently manage real-time distributed control systems, with a high level of security and integrity of transmitted data. A CAN network in its most traditional version is composed of a linear bus, so it is simply a communication channel that allows peripherals to interface with the components of an electronic system, by exchanging information or system data through the transmission and reception of signals [32]. In the test bench a CAN Network at USB 2.0 High-Speed from ESD electronics is used (see Figure 2.9b). Thanks to this element it is possible to send and receive data from the PC to the board and vice versa [33].

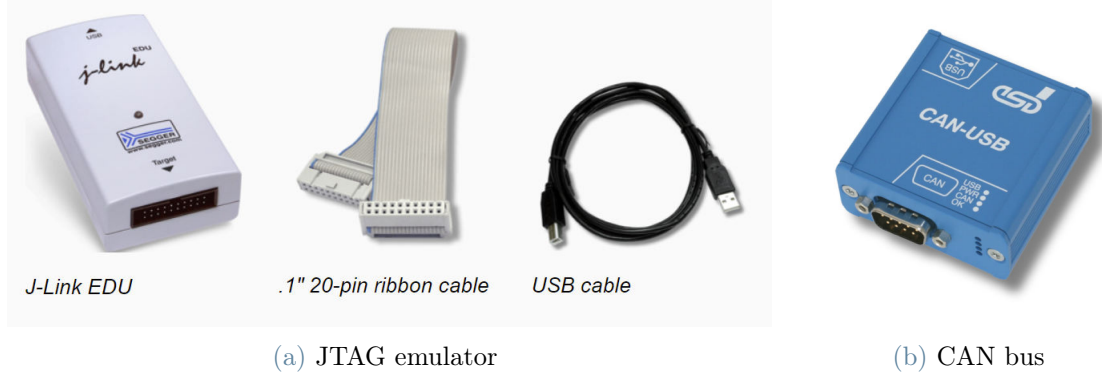


Figure 2.9: Joint-PC connections: the JTAG is used for TWIN firmware, while the CAN bus is used for TWIN software

2.2.2. Control Strategies

As previously mentioned, in both the presentation of rehabilitative exoskeletons and TWIN control strategies, a position control is often used to realize the desired movement. This is not of course the only type of control that can be found. In the case of TWIN and especially in this thesis project, two controllers were considered: a duty-based transparency control and the torque control.

Duty-based transparency control

Transparency measures the robot ability of not applying any assistance/resistance to free motion. Specifically transparency, qualifies the mechanical properties of the structure (weight, inertia, friction, etc.), of its actuation (backdriveability, friction, etc.), and of the performances of the low-level control dedicated to the compensations of these perturbing phenomena (feedforward compensation of the gravity and friction, for example). A lack in transparency can generate undesired resistances during the motion of patients [34].

In more technical terms, a system can be called transparent if the estimated disturbances $\hat{\tau}_{dis}$ can fully compensate for the actual disturbances τ_{dis} : $\tau_{dis} - \hat{\tau}_{dis} = 0$.

In reality, however, a disturbance will never be fully compensated, for example due to noise, communication delay and inertia. Moreover, human-exoskeleton interactions also create disturbances, but these obviously cannot be known in advance. Therefore, the controller has to wait for these interactions to be measured with a force/torque sensor, for example, in order to take them into account [34].

In TWIN a duty-based transparency control computes duty given the angular velocity ω through a feed-forward controller (see Figure 2.10).



Figure 2.10: Duty-based transparency controller. This controller computes duty given ω . The angular velocity is derived from the angular position, that in turn is known thanks to the encoder. Then through the duty value the joint is actuated

Inside the controller block, the duty is computed as follows:

$$\left\{ \begin{array}{l} \text{duty} = A \cdot \sin\left(2\pi f \cdot \frac{t}{\text{steps}}\right), \quad \omega < \omega_{min} \quad (2.1a) \\ \text{duty} = \left(\frac{PWM}{V_{bus}}\right) \cdot \left\{p_0 \text{sgn}(\omega) + k[p_1\omega - p_2 \text{sgn}(\omega)\omega^2]\right\}, \quad \omega \geq \omega_{min} \quad (2.1b) \end{array} \right.$$

where A , f and k are the transparency parameters, selected manually by the user; p_0 , p_1 , p_2 are motor parameters fixed for the specific motor used; ω is the angular velocity and V_{bus} is the source voltage; steps are the sinusoidal steps and PWM is the Pulse Width Modulation period. When considering a digital control, a Pulse Width Modulation (PWM) signal is used to generate an average voltage depending on the Duty Cycle.

$$V_{average} = DutyCycle \cdot V_{bus}$$

PWM is a technique based on the modulation of the Duty Cycle of a square wave defined by amplitude, frequency and DutyCycle. It basically consists in the modulation of the signal by partializing in time the signal itself. This is obtained by activating or deactivating the signal through an electronic switch (e.g. transistor) [27].

All of the above terms in the equation 2.1 are known quantities, also the angular velocity which is derived from the angular position, that in turn is known thanks to the encoder. In the controller there are also duty limits values as a safety measure.

The equation 2.1a represents a sinusoid of amplitude A and frequency f , so if the angular velocity is below the threshold, the duty is a sinusoid. In practical terms this means that when the joint is at rest, the motor oscillates continuously so that it is easier to overcome static friction as soon as the velocity increases. Increasing the amplitude or the frequency of course the oscillations are greater and this makes it easier and easier to overcome static friction.

In the equation 2.1b, however, the duty depends exclusively on the angular velocity and on the parameter k , that is a gain parameter.

Therefore to increase the transparency it is necessary to change the transparency parameters in order to find the right compromise and avoid that the joint is unstable for a too high duty value. A graphical representation of these equations 2.1 can be found in Appendix A.

This control is very intuitive and it works well. Moreover with this type of disturbance compensation, the problem of modeling friction and inertia is bypassed because the control compensate all the disturbances. This controller however does not consider motor current, but it would be interesting to include current in this type of control because the latter is directly related to the torques of the system. For this reason, in the thesis project, also the torque control has been taken into account.

Torque control

Under the assumption of constant magnetic field, it's possible to assume that the torque generated by the DC motor is proportional to the armature current by a constant factor motor torque K_t and to the reduction ratio τ [35]:

$$T = K_t \tau \cdot I \quad (2.2)$$

However, this relation is ideal; it does not take into account dissipations. Simplifying and schematizing the motor-load system as a system of rotating masses as in Figure 2.11, it is clear that the torque expressed by the motor is in the opposite direction than T_r which represents the resistant torque due to dissipation, i.e. inertia and friction.

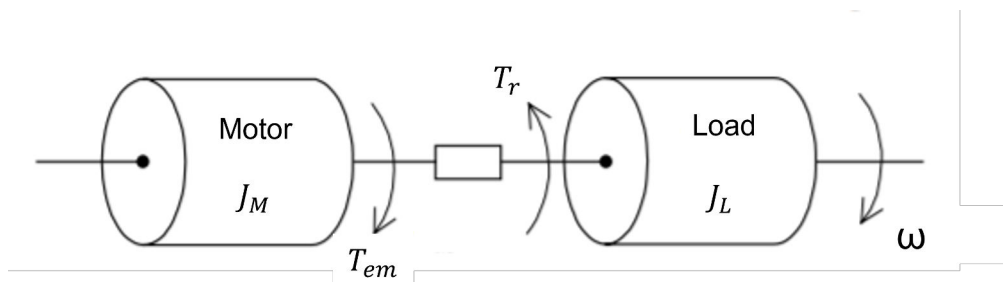


Figure 2.11: Motor-load system

Therefore, real torque-current relation is expressed by the dynamic equilibrium equation for the system (Newton's Law) (2.3).

$$T = T_{electromechanical} + T_{resistant} \quad (2.3)$$

where $T_{resistant} = T_{inertia} + T_{friction}$ [36].

So, explicating the terms, equation 2.3 becomes [37]:

$$T = J\ddot{\theta} + \beta\dot{\theta} + K_t\tau \cdot I \quad (2.4)$$

where:

- $J\ddot{\theta}$ is the torque contribution due to inertia and J is the inertia of the system, hence of the motor system and load ($J = J_M + J_L$);
- $\beta\dot{\theta}$ is the torque contribution due to friction and β is the friction coefficient;
- $K_t\tau \cdot I$ is the electromechanical torque;
- $\theta, \dot{\theta}, \ddot{\theta}$ are respectively the angular position, the angular velocity (ω in Figure 2.11) and the angular acceleration.

Typically the contribution due to $T_{friction}$ is represented by a specific model, as mentioned in Section 1.3.

In the case of TWIN joints, a Coulomb+viscous model of this type was used:

$$T_{friction} = F_v \cdot \omega + F_s \cdot \tanh(40\omega) \quad (2.5)$$

where F_v is the viscous friction coefficient expressed in $\left[\frac{Nm}{rad/s}\right]$, F_s is the static friction coefficient expressed in $[Nm]$.

A graphical representation of (2.5) is shown in Figure 2.12

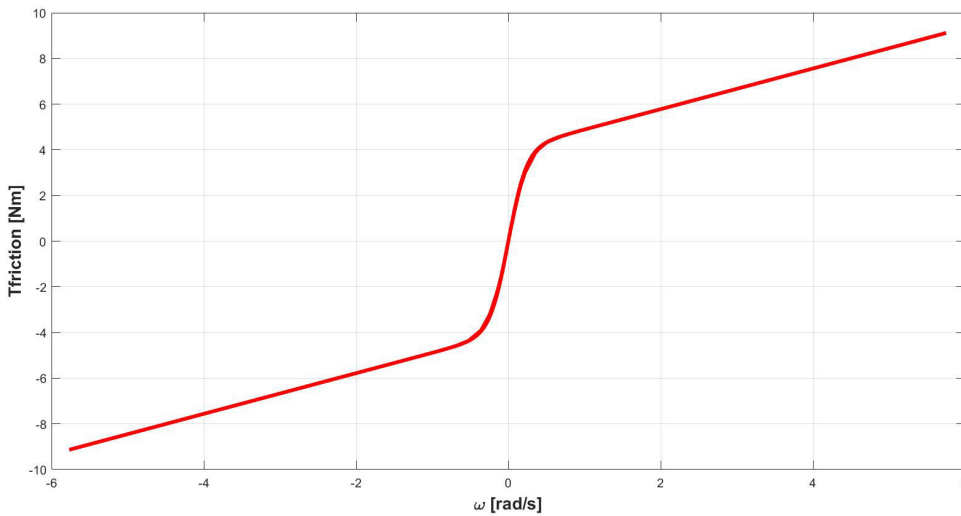


Figure 2.12: Coulomb+viscous model in TWIN joints

The torque controller within TWIN computes the target current I from target torque values, velocity and acceleration input. In fact, the inertial torque and the friction torque generated by compensations are summed to the target torque. Then the current is computed from the total acting torque and it is used to drive the joint (see Figure 2.13).

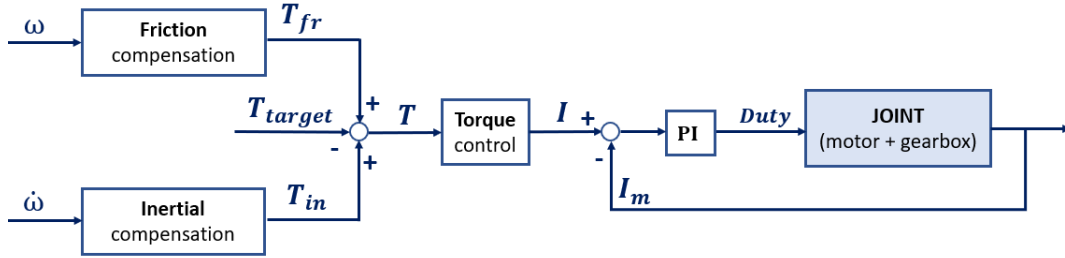


Figure 2.13: Torque controller. This controller computes the motor current given the target torque, the angular velocity and accelerations; then also the motor current is controlled in order to drive the joint.

The motor current is computed as follows:

$$I = \frac{1}{K_t \tau} [T_{target} + T_{inertia} + T_{friction}] \quad (2.6)$$

Combining 2.5 and explicating 2.6:

$$I = \frac{1}{K_t \tau} [T_{target} + J \cdot \dot{\omega} + F_v \cdot \omega + F_s \cdot \tanh(40\omega)] \quad (2.7)$$

where K_t , J , F_s , F_v are fixed parameters, specific for the motor used; T_{target} can be manually selected by the user, if $T_{target} = 0$ the joint works in transparency; ω and $\dot{\omega}$ come from the BLDC Controller data structure, so they are computed from the position, given by the encoder.

To sum up, the torque controller, given input values for angular velocity and acceleration, computes a current. In fact, current limits are set for safety reasons. In addition, every time the torque controller is enabled, a current controller is also enabled. The diagram in Figure 2.13 shows how the motor current is controlled by a PI controller, that takes the $(I - I_m)$ signal as input where I_m is the measured current.

The torque control compared to the duty-based transparency control is based on a physical phenomenon and is very intuitive. The disturbances acting on the system are well distinguished and can be compensated if they are well modeled. The transparency of

the joint can be achieved simply by zeroing the target torque value. Moreover a good knowledge of the acting torques and a good friction compensation by this control allows the development of an impedance control. In spite of these advantages, torque control is present within the TWIN firmware, but it is not used, mainly for three reasons:

- difficulty to manage the current controller;
- difficulty in calculating inertia because of the noise of acceleration;
- difficulty in modeling friction because, as already underlined, friction is a complex phenomenon and it is extremely variable from device to device, and because there are no torque sensors, therefore it is not easy to obtain precise torque measurements.

2.2.3. Testing campaign

According to the considerations done about torque control and being the goal of the thesis the compensation of friction, a testing campaign as been carried out with the purpose of:

1. analyzing the various torque contributions;
2. detecting the torque contribution due to friction;
3. exploiting the torque control already present in TWIN.

The initial idea was to do some tests by attaching different weights (3kg, 2.5kg, 2kg, 1.5kg, 1kg) to the joint's rigid link (see Figure 2.15). In fact, setting the link to an initial known position with the weight attached and enabling the duty-based transparency control, the link lowers until it reaches the stop (the shaft is stopped by a mechanical stop that avoid hyper-extension).

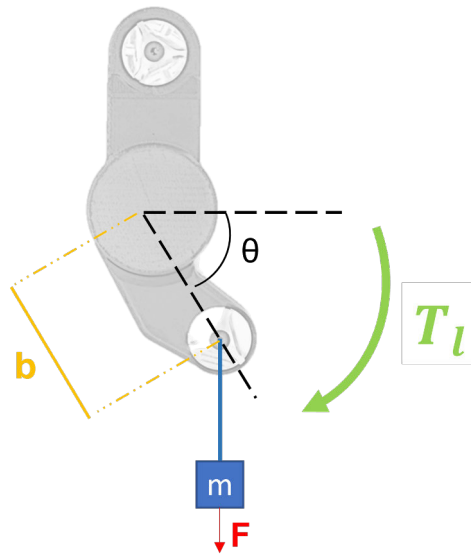


Figure 2.14: Load torque acting on the joint. The figure shows the weight force and the resulting load torque

Knowing therefore the weight force F , the length of the shaft b , the variation of position θ (see Figure 2.14), it is possible to find the load torque:

$$T_l = F \cdot b \cos\theta \quad (2.8)$$

At the end of the test, once the control is disabled, a .log file containing information about the measured variables was automatically saved. In particular, in the .log file there were data related to: time, position, target position, measured current, target current, voltage bus, target torque, velocity and duty.

Of course before enabling the control, the transparency parameters, A , f and K , were set, following a specific protocol. The direct experience, i.e. manually moving the link, led to the identification of ideal K values, so $K = 1$, $K = 1.10$ and $K = 1.15$.

Values of K lower than 1 have not been considered because the link moved with extreme difficulty, while values higher than 1.15 have not been considered to avoid the instability of the system; the risk was in fact that the link moved too fast without control.

Then doing random tests, it was noticed that the ideal frequency is around 3 Hz and therefore it was kept fixed. The frequency in fact not only has no decisive contribution, but also it should not be too high otherwise it may happen that the amplitude fails to reach the set peak value. So, in order to avoid this kind of problem and being the frequency not very relevant, it was decided to keep it fixed.

The amplitude parameter instead varied a lot, because it was considered more relevant.

Parameter A varies from 140 to 195 according to the type of weight, so for heavier weights the chosen amplitudes have values close to 140 and vice versa for lighter weights the chosen amplitudes have values close to 195. This is quite obvious thinking about the meaning of the parameter A.

Five different weights were chosen and 9 tests were performed for each weight, thus a total of 45 tests. At the end of each trial, the .log file was saved and processed in Excel and then later exported in MATLAB for in-depth analysis. The Figure 2.15 shows the weights and the set up used for the testing campaign.

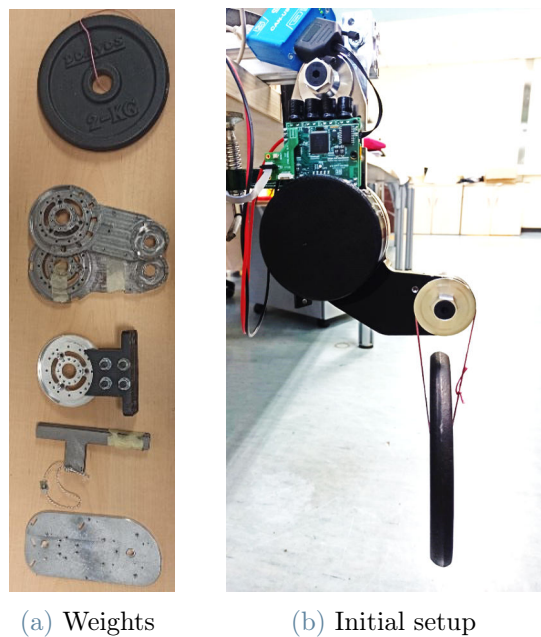


Figure 2.15: Weights and test bench used during the testing campaign

2.3. Friction model

2.3.1. Analysis

After extracting the vectors for time and position, time was normalized by setting the first value of the vector to 0 seconds and angles were also normalized by setting the first value of the position vector to 90° . Note that in the .log file the time is expressed in seconds [s] and the position in radians [rad]. After that, the torque was computed according to the relation 2.8. This type of analysis was performed for each weight and the graphic results can be found in Appendix B.

Post-processing

In addition, for better analysis, post-processing of angular speed and acceleration was performed, which are important measurements for model development. It is often useful to decompose a sequence of N samples into a number of sub-sequences $M \leq N$ by means of M band-pass filters whose central frequencies are appropriately offset and whose pass bands (called subbands) are not necessarily equal to each other. The subband decomposition allows to approach the situation where the signal spectrum is uniform in each subband. A very important requirement of subband decomposition is that of perfect re-composition, so a decomposition system in cascade with a re-composition system gives the starting signal without holes or peaks in the transfer function and with the complete cancellation of the equivocation disturbance, generated by the downsampling of the subbands [38].

For these reasons, downsampling was first used to reduce the sampling rate of the signal. The rate reduction of an integer factor M means to decimate the filtered signal by M ; that is, keep only every M^{th} sample.

Subsequently a moving average filter was applied. A moving-average filter is a common method used for smoothing noisy data. To do this, the filter, with a window of length *windowSize*, slides the window along the data and computes the averages of the data contained in each window. The following difference equation defines a moving average filter of a vector x :

$$y(n) = \frac{1}{\text{windowSize}}(x(n) + x(n-1) + \dots + x(n - (\text{windowSize} - 1))) \quad (2.9)$$

The vector $y(n)$ is the new vector filtered [39].

These two techniques are easy to implement in Matlab, while it is difficult to find suitable values for M and *windowSize* that do not cause too much delay or lose too much information.

In this analysis, the angular velocity obtained directly from the .log file create a signal with a frequency of 1000Hz filtered first with a downsampling of 10 and then with a moving average filter with a window size of 10. The angular acceleration $\dot{\omega}$ instead was derived by doing the discrete derivative of ω using the forward difference method [40]:

$$\dot{\omega}(i) = \frac{\omega(i+1) - \omega(i)}{\Delta T} \quad (2.10)$$

The post-processing results are shown in Section 3.1.

2.3.2. Modeling

The results of the analysis conducted are the load torque values. At this point it is possible to obtain the friction torque in an indirect way taking into account the torques acting on the joint (see Figure 2.16).

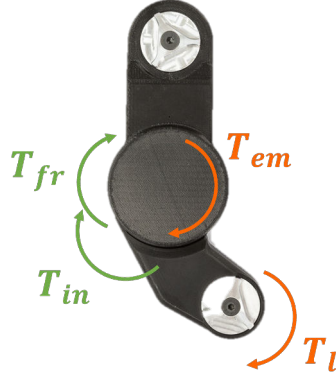


Figure 2.16: Joint' torques: the orange arrows are the load and electromechanical torques, the green ones are the dissipation torques

Recalling in fact equation 2.3 and making explicit the friction torque T_{fr} , the following relation is obtained:

$$T_{fr} = T_{rm} + T_l - T_{in} \quad (2.11)$$

It is useful to remember that:

- $T_{em} = K_t \tau \cdot I$,
is the electromechanical torque, where K_t is known from the motor data-sheet and I is the target current given by the .log file;
- $T_l = F \cdot b \cos \theta$,
is the load torque and is obtained with the analysis described in 2.3.1;
- $T_{in} = J_{system} \cdot \dot{\omega}$,
 $J_{system} = J_{motor} \cdot \tau^2 + J_{gearbox} + J_{link} + J_{mass}$
is the inertial torque, where J_{motor} and $J_{gearbox}$ values can be found in the data-sheet of the motor and of the harmonic drive, J_{link} can be derived from the CAD of the joint, while $J_{mass} = m \cdot b^2$.

Combining all these terms the friction torque is obtained:

$$T_{fr} = K_t \tau \cdot I + F \cdot b \cos \theta - [J_{motor} \cdot \tau^2 + J_{gearbox} + J_{link} + J_{mass}] \cdot \dot{\omega} \quad (2.12)$$

Now that the contribution of friction torque for each weight is known, it is necessary to find the model that describes this data.

The Curve Fitting Toolbox of Matlab is used in order to create a model that fits all the data. To select data to fit, the variables from MATLAB workspace are chosen (X data and Y data, that in this case are ω and T_{fr} respectively because the friction torque is a function of the angular velocity). After selecting the variables, the Curve Fitting app immediately creates a curve with the default settings. The fit can be refined changing fit type or creating a custom equation. With the graphical method is possible to evaluate the goodness of fit, but it is also possible to examine the goodness-of-fit statistics. Curve Fitting app in fact computes the following values [41]:

- *SSE* is the sum of squares due to error of the fit. A value closer to zero indicates a fit that is more useful for prediction;
- *R-square* is the square of the correlation between the response values and the predicted response values. A value closer to 1 indicates that a greater proportion of variance is accounted for by the model;
- *Adjusted R-square* is the degrees of freedom adjusted R-square. A value closer to 1 indicates a better fit;
- *RMSE* is the root mean squared error. A value closer to 0 indicates a fit that is more useful for prediction.

The model chosen to represent the friction is that of the *rotational friction*, so a model that takes into account the contribution of Coulomb+viscous friction, but also the Stribeck effect. This choice had already been hypothesized by the study of the literature and then it was also confirmed experimentally on the basis of the results obtained from the testing campaign. The friction torque for each of the different weights, showed in fact a trend similar to that in Figure 2.17.

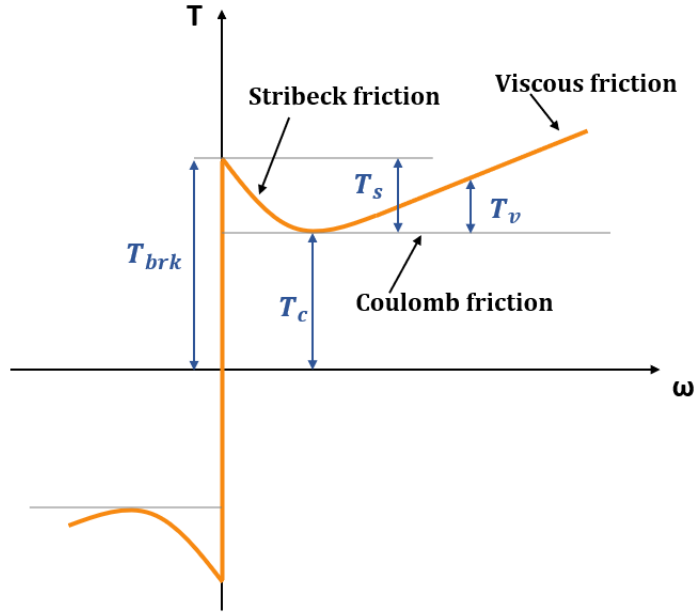


Figure 2.17: Rotational friction model with the different friction effects [42]

T_s is the Stribeck friction, taking place at low velocities; T_c , the Coulomb friction, is a constant torque at any velocity, while the viscous friction, T_v , is directly proportional to the relative velocity ω . T_{brk} is the breakaway friction. The total friction is approximated with the following equations [42]:

$$T = \sqrt{2e}(T_{brk} - T_c) \cdot \exp\left(-\left(\frac{\omega}{\omega_{St}}\right)^2\right) \cdot \frac{\omega}{\omega_{St}} + T_c \cdot \tanh\left(\frac{\omega}{\omega_{Coul}}\right) + f\omega, \quad (2.13)$$

$$\omega_{St} = \omega_{brk}\sqrt{2}, \quad (2.14)$$

$$\omega_{Coul} = \omega_{brk}/10. \quad (2.15)$$

Where ω_{brk} is the breakaway friction velocity, ω_{St} is the Stribeck velocity threshold, ω_{Coul} is the Coulomb velocity threshold and f is the viscous friction coefficient. The results of the modeling are in Sections 3.2, 3.3 and 3.4.

2.3.3. Compensation

Once the friction model has been found, it needs to be tested on the joint.

The implementation of the model goes through three sub-stages:

1. implementation on the TWIN's firmware of the filtering method;

2. inserting the new model relation in the TWIN's firmware;
3. configuration of the torque control on the TWIN's software.

1. Filtering method

This first step is performed within the firmware, that has been developed in Eclipse. Eclipse is an integrated development environment (IDE) used in computer programming. It contains a base workspace and an extensible plug-in system for customizing the environment. Eclipse is written mostly in Java and its primary use is for developing Java applications, but it may also be used to develop applications in other programming languages via plug-ins, including C [43], that is the language used. The changes were made within the main code, in the system tick handler function. This function is activated every 1ms, with a frequency of 1000Hz. In order to downsample and take a speed value with a frequency of 100Hz, inside the system tick handler function the tick counter is analyzed every 10ms. Then the angular velocity ω is calculated instant by instant and a moving average filter of window size of 10 is applied.

2. Import the model

The friction model is imported within the torque control code. Moreover a gain parameter G has been introduced to regulate the friction compensation percentage (it goes from 0 to 1), as expressed by the equation (2.16).

$$I = \frac{1}{K_t \tau} [T_{target} + T_{in} + T_{fr} \cdot G] \quad (2.16)$$

3. Configuration of torque control

The configuration of the torque control was done within the software code, in Qt Creator. Qt Creator is a cross-platform C++, JavaScript and QML integrated development environment which simplifies GUI application development [44]. Changes were made in the Can Board code to read the message strings so that the correct torque control variables were taken. Also the Can Board Monitor code was modified by adding the user interface in order to adjust the torque control manually as well. With the following modifications in fact it is possible to enter in the torque control interface, enable and disable the control and manually change the target torque values (add or decrease by 0.05). By default the target torque is set to 0, in order to have a total friction compensation and a transparent movement.

Model validation was done with a comparison of motor currents, and root mean square

error was used as evaluation metric:

$$RMSE = \sqrt{\frac{1}{N} \sum_{i=1}^N (y_i - x_i)^2}$$

where y_i is the estimated value (target current), x_i is the effective value (measured current) and N is the number of samples. Model validation results are described in Section 3.5.

2.4. Impedance control

Friction compensation is performed employing the torque controller, in which it was also possible to realize a preliminary design for an impedance control. A definition of impedance and impedance control was given in Section 1.4, which can be summarized in Figure 2.18.

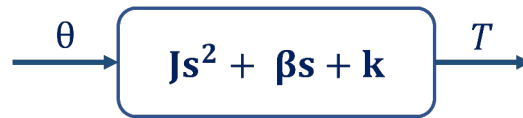


Figure 2.18: General impedance control: the input is the actuator position and the output is the desired torque. Inside the block impedance is assimilated to a generalized mass-spring-damper system.

In TWIN there is the possibility to implement this kind of control, in fact, thanks to the encoder, the position values are known instant by instant. A description of this controller is in Figure 2.19.

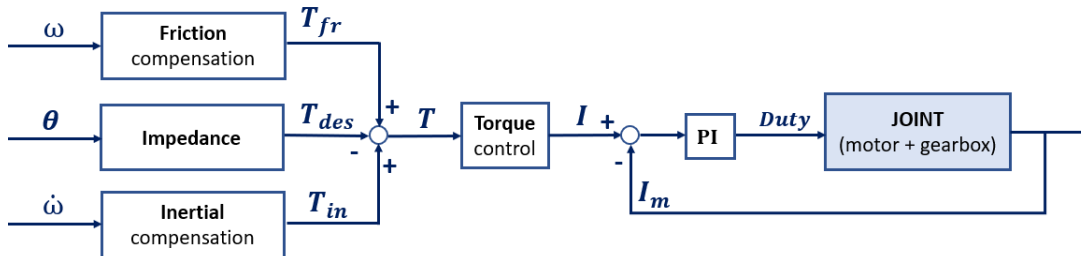


Figure 2.19: TWIN impedance controller: the exoskeleton is capable of measuring θ actuator positions and imparting a desired torque through an impedance control. Then the torque controller, given also the friction torque and the inertial torque, computes the motor current to drive the joint.

For simplicity and to verify that this control actually works, only the contribution of the spring was considered, so the torque T_{des} is directly proportional to θ position by a factor of k , i.e., a stiffness, in particular:

$$T_{des} = k(\theta - \theta_0) \quad (2.17)$$

where θ_0 is the initial position. When the joint moves away from its initial position, exactly as happens in a spring, a recall torque is exerted proportional to the displacement from the initial position, according to stiffness k .

It remains at this point to implement the relation 2.17 inside the torque controller. The question that arises is how to choose these parameters:

- θ_0 can be chosen arbitrarily. The knee joint has an angular excursion ranging from 122° to -4° therefore an intermediate measure of 60° was chosen in order to verify that a torque is exerted in both positive and negative directions.
- in order to choose instead the parameter k some tests have been made with the control implemented in the equation 2.16. Experimentally at about 20° a torque of $1Nm$ was generated and therefore being the spring linear, the slope is $k = \frac{1Nm}{20deg} = 0.05 \frac{Nm}{deg}$ (see Figure 2.20)

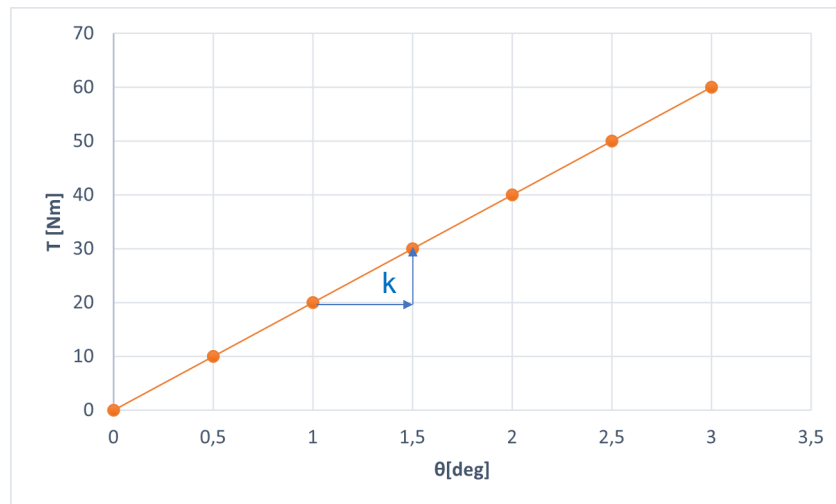


Figure 2.20: Linear stiffness. The torque over the angular position shows a linear trend with slope k , because only the spring contribution was considered

Once the parameters have been chosen, the torque contribution has been implemented in

the torque controller, in the following way:

$$I = \frac{1}{K_t \tau} [T_{in} + T_{fr} \cdot G - T_{des}] \quad (2.18)$$

where T_{des} is the impedance torque, i.e. that of equation 2.17. Results about the impedance control application are described in Section 3.6

Obviously within the control the appropriate conversions have been made in order to go from position degrees to radians and then to ticks.

To improve the graphical interface, three controls have been added to the Can Board Monitor:

- a control called *friction control* that acts like the transparency control and is represented by equation 2.16 without the contribution of target torque.
- a control called *torque control*, represented by equation 2.16, in which it is possible to manually choose the target torque value.
- a control called *impedance control* that is represented by equation 2.18. From the monitor it is possible to choose manually the value of k and θ_0 .

2.5. Hip and knee joints

In light of the results obtained, the thesis project involved the addition of a hip joint in order to have a complete description of the leg motion. In fact the hip and knee are the two actuators (recall that the ankle joint consists of an AFO).

The experimental setup was almost the same as for the knee joint. The only difference between the two test benches is that the hip joint consists of a Maxon EC90 motor with a nominal voltage of 36V. This results in different K_t and J_{system} values. The weights used for the testing campaign were also the same and the same testing protocol was performed. Once the data was collected, a model for friction compensation was implemented. The steps were the same as for the knee joint: torque analysis, modeling of friction torques, compensation. Refer to Section 2.3 for the methodology used, and to Sections 3.3 for the results on the hip model. Impedance control was then implemented for the hip as well.

At this point, the hip and knee joints were physically connected via a link, representing the femur, to perform tests on the entire leg and to verify that the models created would also work on a test bench of greater complexity. The final test bench is shown in Figure 2.21. For the sake of simplicity and not to modify the software part, a second CAN was

added.

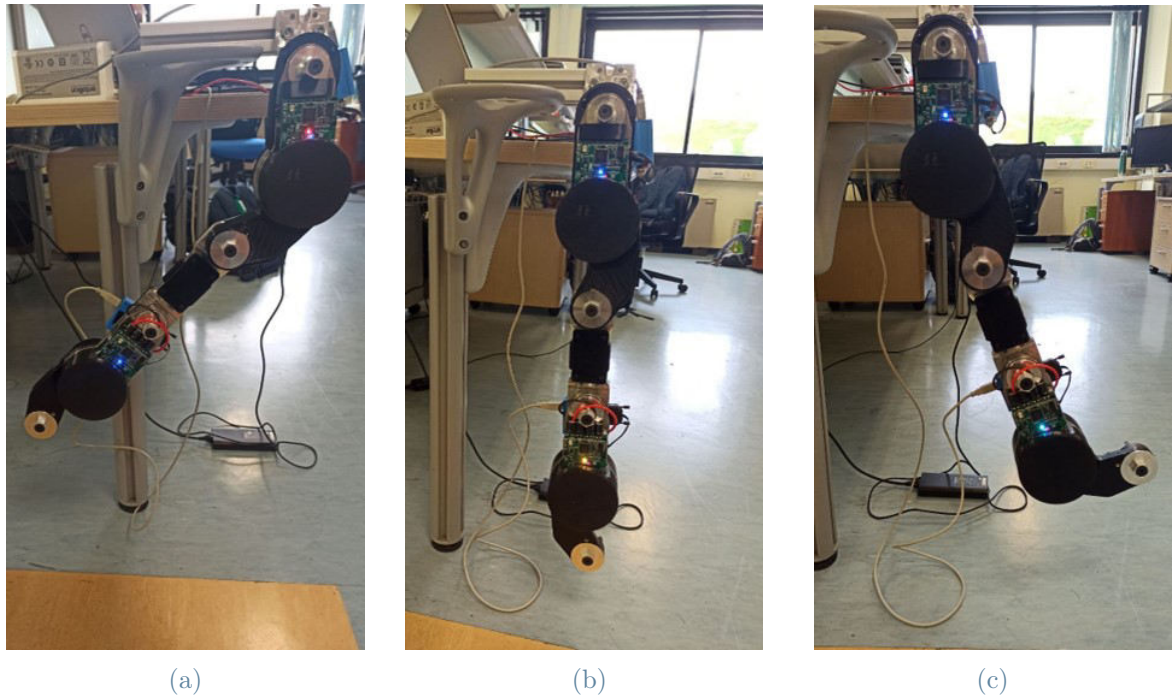


Figure 2.21: Leg test bench with hip and knee joints connected through a rigid link representing the femur. In the three figures a flexion-extension of both hip and knee can be appreciated.

3 | Results

This chapter collects the results obtained from the experiments described so far. In Section 3.1 the post-processing results are shown, while in Sections 3.2, 3.3, 3.4 the friction compensation models for the hip joint and the knee joint are presented. Section 3.5 describes the validation of the models and finally the results obtained from the impedance control tests are shown in Section 3.6.

3.1. Post-processing

As previously described in Subsection 2.3.1, post-processing was performed within the firmware to filter the velocity ω . The results of the filtering are shown in Figure 3.1, derived after a joint motion test, that represents the angular velocity trend over time. The angular velocity ω (blue) was first filtered with an undersampling of 10 to reduce the sampling rate of the signal. This reduction is shown by the red ω_{US} signal. In order to make the signal even smoother, a moving average filter with a window size of 10 was applied, as shown in the yellow ω_F signal. From the Figure 3.1 we can also see a delay of about 0.5 seconds between ω and ω_F , due to post-processing.

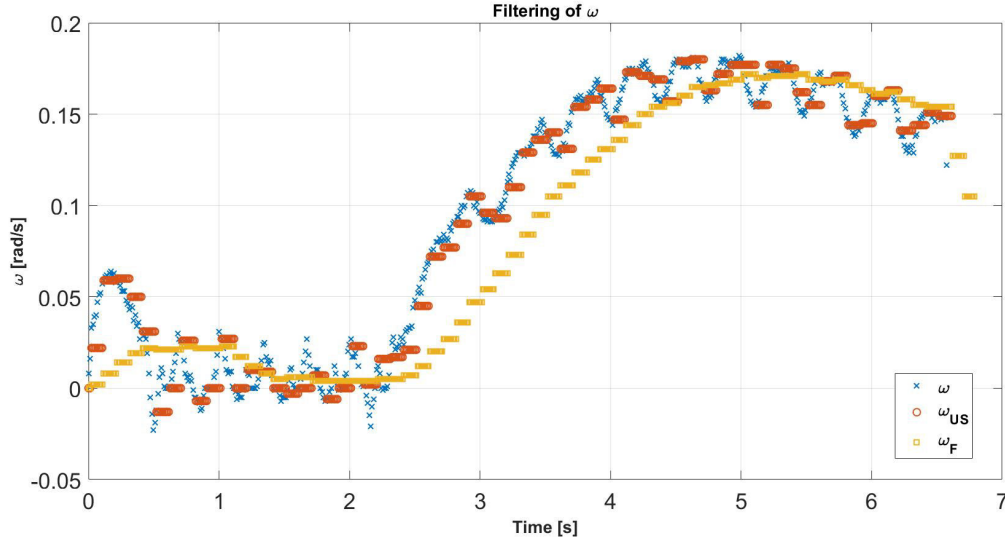


Figure 3.1: Post-processing of the angular velocity. The figure shows the angular velocity over time after a joint motion test: the blue curve is the original signal of the angular velocity, the red one is the velocity after the undersampling and the yellow one is the signal filtered with the moving average filter.

3.2. Knee model

In Subsection 2.3.2, the procedure to create a model for friction compensation was described. The tool used is the Curve Fitting Toolbox of MATLAB. After entering the data into the toolbox, the fitting was refined with a custom equation. The equation chosen to model the friction is 2.13. After entering these equations into the Curve Fitting Toolbox, with appropriate parameter adjustments, it turns out that the friction torque data are represented by the following model:

$$T_{fr} = \sqrt{2}e(a - b) \cdot \exp\left(-\left(\frac{\omega}{c\sqrt{2}}\right)^2\right) \cdot \frac{\omega}{c\sqrt{2}} + b \cdot \tanh\left(\frac{\omega}{c/10}\right) + d\omega, \quad (3.1)$$

where a, b, c, d are parameters generated by the toolbox. The first term, exponential, is the Stribeck contribution; the second term represents the static friction and is given by the coefficient of static friction b , multiplied by a hyperbolic tangent, whose peculiar trend avoids singularities at the origin; the last term instead represents the viscous friction and is given by the coefficient of viscous friction d , multiplied by the angular velocity ω . The model 3.1 is represented graphically in Figure 3.2 that describes the friction torque T_{fr} over the angular velocity ω .

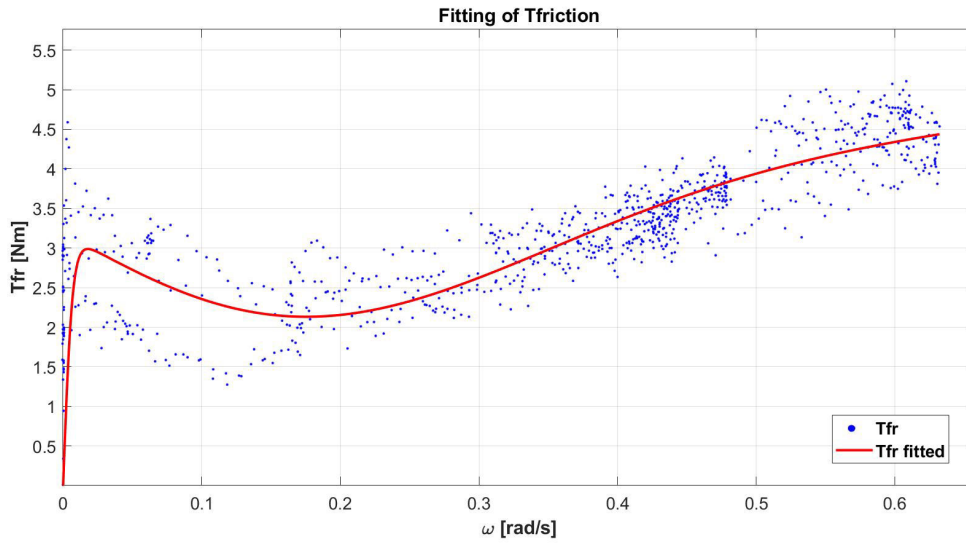


Figure 3.2: Knee friction compensation model. The red curve is the model that fits all the blue data, which are the friction torques of the different weights.

The Curve Fitting Toolbox moreover gives the statistical indices in order to estimate the goodness of the fitting: $R^2 = 0.3936$, $AdjustedR^2 = 0.3916$. Although the values of R^2 and $AdjustedR^2$ are far from the unit and so the model does not fit strongly to the data, graphically it is evident that the red curve represents well the data trend. The cause of such values is to be attributed to an initial dispersion of the data. The indices related to a predictive analysis have not been considered.

3.3. Hip model

In order to obtain the friction compensation model related to the hip joint, as for the knee joint, equation 2.13 was implemented into the Curve Fitting Toolbox, adjusting parameters a, b, c, d appropriately. The model for the hip is represented graphically in Figure 3.3 that describes the friction torque T_{fr} over the angular velocity ω .

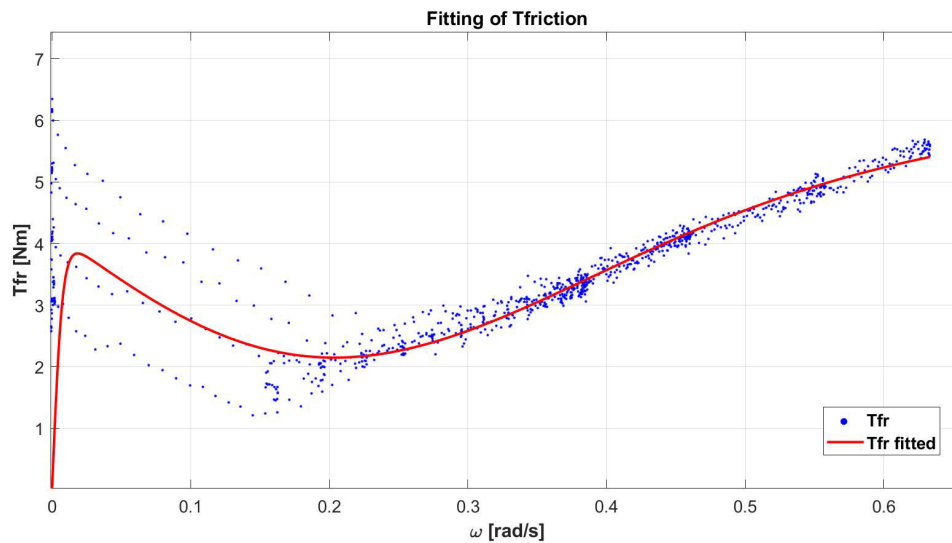


Figure 3.3: Hip friction compensation model. The red curve is the model that fits all the blue data, which are the friction torques of the different weights

Again, the R^2 and $AdjustedR^2$ values are far from unity, even negative, and indicate a very weak fit ($R^2 = -0.446$, $AdjustedR^2 = -0.4505$). The cause is the large variance in the data, as can be seen in the initial part of the red curve, where the Stribeck effect is strongly dependent on the applied load. However, as in the knee joint, graphically it can be seen that the red curve represents well the data trend as the velocity ω increases. Indices related to a predictive analysis were not considered in this case either.

3.4. Hip and knee models

A comparison plot between the two models is shown in Figure 3.4

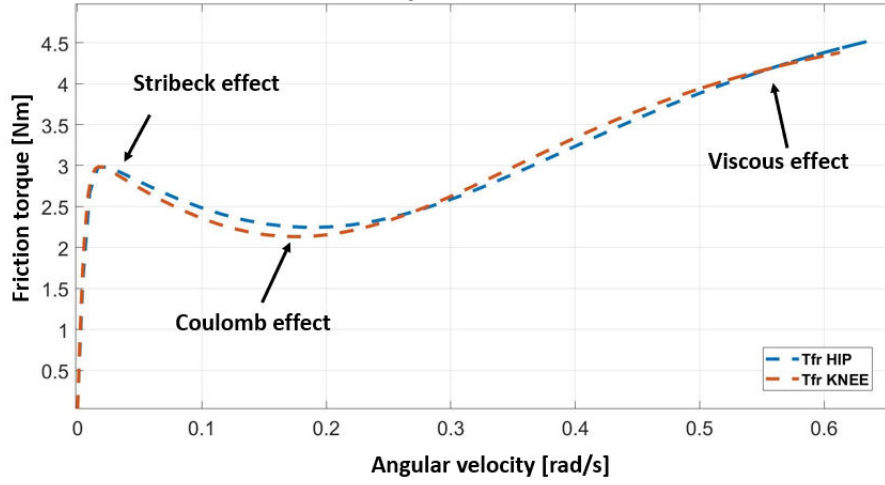


Figure 3.4: Hip and knee friction compensation models: the dashed blue line is the hip friction torque while the dashed red line is the knee friction torque. In the figure the different friction effects can be appreciated.

It is evident how the two graphs differ only for the Stribeck and the Coulomb effects. Other differences between the two models are the parameters a, b, c, d , as shown in the Table 3.1.

Parameters	Knee	Hip
a	-1.743	1.664
b	-3.193	4.2
c	-0.2031	0.2252
d	2.06	2.26

Table 3.1: Models' parameters created with the Curve Fitting Toolbox.

3.5. Model validation

Once the models for the hip and knee joints were obtained, they were implemented within the firmware and software, as described in Subsection 2.3.3. In order to get a validation that the models are working, the measured current value I_m was compared to the target current value, i.e. the torque control output I . As an example, the results for the currents in the knee joint are depicted in Figure 3.5 that describes the currents trend over time.

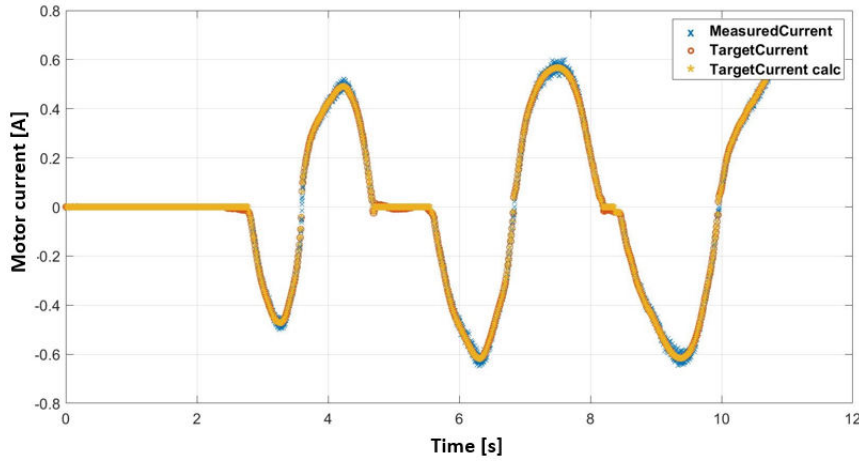


Figure 3.5: Motor current values comparison in the knee joint. The measured current is the blue line, the target current is the red line. As validation the yellow line is the numerical target current computed with a MATLAB simulation.

In the chart, an overlap of measured current and target current is evident ($RMSE = 0.0113A$), a proof that the torque control is working well. The yellow curve is instead the numerical target current computed with a MATLAB simulation after the test and it is overlapped with the target current I ($RMSE = 0.0035A$). This means that the model implemented in MATLAB has been correctly imported into the TWIN firmware.

3.6. Impedance torque

As anticipated in Section 1.4 the impedance was modeled with a spring having stiffness k . The implementation of impedance control produced the results shown in Figure 3.6, where the trends of electromechanical torque T_{em} and impedance torque T_{des} over angular position are described. The test was performed by moving the joint in one direction far from initial θ_0 and then in the opposite direction.

The linear behavior of T_{des} (red line) can be noticed, whose trend follows perfectly the line with slope k .

The spring effect of T_{em} (blue line) can then be deduced. Zone 1 of the graph represents the torque when the joint is moved downwards, exactly as when a spring is pulled and moved far from the initial equilibrium point. In this case the torque tends to return with the same trend to the position θ_0 , set to 0° . Zone 2 of the graph represents instead the torque when the joint is moved upwards, like when a spring is compressed. Also in this case the torque returns to the position θ_0 with the same trend and opposite direction. The T_{em} trend has a correct torque-angle slope ($K = 0.0493 \frac{Nm}{deg}$, found this time in MATLAB

with a simple linear regression [45]), very similar to the torque-angle slope of T_{des} and this is an index of the correct reproduction of the desired stiffness, but a not negligible hysteresis is present, probably due to the not complete compensation of the viscous effects inside the joint.

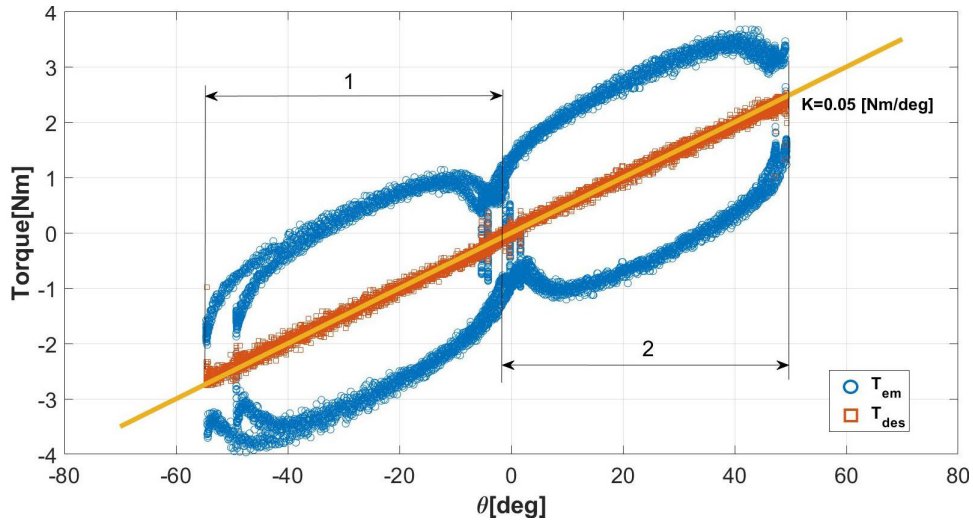


Figure 3.6: Trend of electromechanical torque (blue line) and impedance torque (red line) over angular position. K is the stiffness and is represented by the straight yellow line and θ_0 is set at 0°

Figure 3.7 shows again the contributions of T_{des} and T_{em} over angular position, on the same type of test (joint pushed down), but with different compensation percentages, i.e. $G = 35\%$, $G = 40\%$, $G = 45\%$. As the compensation percentage increases, the spring effect is more and more exasperated, in fact, a progressive increase of the oscillation around the equilibrium point θ_0 can be noticed. At higher values of G , there is also a higher amplitude of the curves, consequently a greater hysteresis and therefore an increase of the dissipated energy.

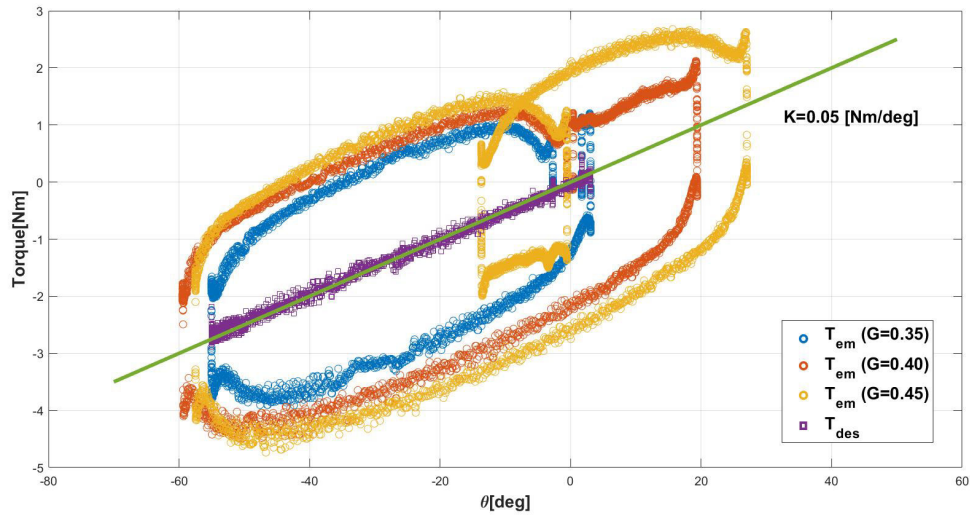


Figure 3.7: Trend of electromechanical torque and impedance torque (purple line) over angular position with different friction compensation. K is the stiffness and θ_0 is set at 0° . The blue line is the electromechanical torque with a friction compensation of 35%, the red line is the electromechanical torque with a friction compensation of 40% and the yellow line is the electromechanical torque with a friction compensation of 45%.

4 | Discussion

The aim of the present study was to demonstrate that in order to compensate for friction inside an electromechanical joint, a torque transducer is not necessarily needed, but with a suitable and well representative model of the complex phenomenon of friction, satisfactory results can be obtained. Above all, this model-based approach can also lead to new implementations as in the case of impedance control. The creation of a model for both the knee joint and the hip joint, started from some tests made on the joints with the aim of collecting and analyzing data. The data collected were obviously in raw form, especially data related to natural quantities, so they had to be filtered properly otherwise the analysis could not proceed. In 3.1 is shown the result of a post-processing performed on the angular velocity. A small time delay is present between the original and the filtered signal. Despite this time gap, the signal is still free of noise, it does not lose information and, especially from direct experience, the joint did not perceive the delay, so it performed a clean movement and proceeded unobstructed.

After post-processing the collected data were ready to be analyzed: a first in-depth analysis on load torque and desired transparency was performed and the results are in the Appendix B. This analysis allowed a complete understanding of the phenomena acting on the test bench. Next, after finding the torque contributions of the friction indirectly, they were analyzed with appropriate curve fitting tools. The resulting models were presented in 3.2, 3.3, for the knee joint and hip joint, respectively.

The statistical indices of these models indicate a very weak fit, but the cause is in the high initial data dispersion. Further tests to collect more data, would be necessary to improve the performance of the models and the statistical indices.

In Section 3.4 for the sake of completeness, the two models are compared: the difference between them is not very relevant, it can be perceived only by analyzing the parameters of the models. It is clear that, despite the complexity of the phenomenon of friction, these trends are well represented by a rotational friction model, in which the recurring elements are the Coulomb effect, the viscous effect and the Stribeck effect.

In order to get a complete overview of how friction acts at joints it would be appropriate to

look at the behavior of friction over time. The joints used in this study were fairly recent and therefore did not yet suffer from time dependence. In the very first test bench used in this thesis project, which has not been presented because it was a simple attempt and a first approach to the device, the behavior of friction was different, it did not take into account the Stribeck effect and was very similar to the friction model already present in TWIN (equation 2.5). It is important to specify that this test bench was not a real joint, but consisted of the same electrical and mechanical components. However, despite the similarities of the components, the friction model of this test bench was strikingly different. This doesn't imply that the models implemented in this study cannot be replicated in the various TWIN exoskeletons because the friction changes as the devices change, but it must be kept in mind that the friction phenomenon is complex. Therefore, a model-based approach to friction compensation is a simple, cost-effective solution with great potential, but having a torque transducer that measures torque allows a view over time of the friction variations. In a device such as an exoskeleton that is assumed to offer high reliability over time, this aspect must be considered. Alternatively, predictive models can be used, but they are difficult to implement.

Another aspect related to friction that has not been investigated is the effect of temperature. The joints of exoskeletons do not work at high speeds, but they work for a long time if we consider their use in rehabilitation structures. Inevitably this leads to an increase in temperature at the level of the joints. In fact, it would be optimal to understand how friction varies as temperature varies, by performing tests and using, for example, thermal imaging cameras.

After creating the models, they were tested in the joints by enabling the torque control. In the Section 3.5 the results concerning the functioning of the models are reported and it is immediately noticed a superimposition of the currents.

This almost perfect superposition, however, hides an overcompensation, which can be appreciated only in practical tests. In fact, the joint tends to be strongly unstable because the current supplied is too high. Therefore it becomes important to add the parameter G , that is the compensation percentage. The minimum value of G has been set to 20% and the maximum to 60%. Setting a proper G parameter, the joint moves in a more controlled way and the resulting motion is definitely transparent.

Another consideration made in the model validation step was about the inertia. At high speeds the joint was acquiring higher and higher accelerations and was difficult to manage, so hard that a forced stop was required for safety reasons. Investigating the problem, it was realized that the accelerations were too noisy and, even with an appropriate filtering, the instability problem recurred, this time however for the excessive

delay caused by the filtering. So the contribution related to inertia was not included, since it is not a fundamental contribution considering the speeds and loads used in the thesis project. However, the contribution of inertia is no longer negligible as the complexity of the structure increases, as in a complete exoskeleton.

It would be interesting to employ accelerometers in order to have a precise measurement of the acceleration and then use this values within the models created. It would be sufficient to put an IMU on the joints used and perform the same tests.

The results are however satisfactory because transparency has been achieved. Moreover, the improvements performed in the graphical interface make it very easy to enable the torque control and to choose the parameters. These results make the torque control very competitive with respect to the duty-based transparency control that does not take into account the current, but simply relies on the duty value. However, during the design development period, several times the joint had slowed motions. It seemed almost that the current slowed down the movement.

At this point the current control was investigated because it is directly connected to the torque control (they are activated together). After many attempts, it was obvious that the current control doesn't work well because the current measurement used to close the control loop I_m , is very noisy, making the control unstable and difficult to use. The problem arises from the fact that the current control of a six-step motor is not easy. It is possible selecting well which of the phases to read, but still there are uncertainties and inaccuracies not easily to bypass.

In the six-step motor, given phase current references, these are compared directly with the measured currents, and the resulting error is the input to the PI controller. The disadvantage of this operating scheme is that the PI controller, operating at steady state with sinusoidal and not continuous quantities, has a non-zero error, therefore is difficult to manage [46]. So considering all this, the problems found are in line with the type of motor used and confirm that the torque control has been configured well, while the problem lies totally in the current control.

The most immediate solution to this problem is to filter the current measurement before using it in the control, and this could provide an improvement in current control (necessary for torque control to work). However, this solution, being a filtering, has the consequent effect of changing the dynamics of the quantities to control and a consequent worsening of the control. Alternatively it would be possible to use a torque control that defines directly a duty value, ignoring the current. This would introduce the problem that the duty is not directly associated to the current and therefore with the same duty different torque behavior could arise.

Another solution would also be to use a different inverter such as Trinamic ones. Trinamic stepper drivers allow to have better control of the stepper motors and achieve extremely quiet motion. The way the driver handles the motor current can be influenced as well as the way the current is delivered [47].

In section 1.4 a preliminary design of an impedance control was discussed, thanks to the model-based approach used to compensate for friction and the implementation of a functioning torque control. The results were presented in 3.6.

From these results, it is clear that in order to have an optimal impedance and transparency, a 35% of friction compensation is required. With this percentage of compensation in fact, the hysteresis is minimized. Impedance control was validated in the same manner for the hip joint, showing the same results.

The last step of the thesis project, included the implementation of the impedance control on the whole leg (hip-femur-knee test bench). The control works properly, obviously setting a G_{knee} different from G_{hip} . In particular it is necessary to set $G_{hip} < G_{knee}$ because the geometry of the test bench changes: the weight of the femur and knee increase the torque applied to the hip and facilitate the compensation of friction. The motion of the entire leg was found to be smooth and controlled. These satisfactory results bode well for a future implementation that also takes into account the damping contribution.

5 | Conclusions

The conclusion that can be drawn from this project is that an exoskeleton to work in transparency needs a good compensation of friction and inertia.

In the TWIN exoskeleton a duty-based transparency control is exploited to compensate friction, but a possible torque control is not investigated, it is only theorized and not implemented.

In this study, therefore, the torques acting on the TWIN joints has been examined in order to understand the system disturbances. The methodology adopted is a model-based approach. The great usefulness of creating a model to describe a complex phenomenon such as friction, has been demonstrated in this thesis project. The strength of this approach lies also in the fact that it is based on a very simple intuition, that is to carry out simple load tests to analyze the loads effect on TWIN joints. This intuition made it possible to have access to a large number of data that, after a proper analysis, led to the creation of realistic friction compensation models. It should also be remembered that this modeling was done without the use of torque or acceleration sensors.

In order to validate the model, a torque controller was enabled. This controller not only performs a friction compensation by working in transparency, but also allows the generation of a target torque.

Moreover, the model development and the implementation of a torque controller allowed the realization of a preliminary design of an impedance control, fundamental in rehabilitative exoskeletons in order to have a realistic replication of the human gait . The design is just preliminary because it does not take into account some phenomena such as damping, so the impedance control should be deepened and modeled totally.

Inertia should then be analyzed for a complete overview of the disturbances acting on the device.

In conclusion, the results of this study are satisfactory and the technical limitations can be easily resolved. Thus, this study led to a very effective friction compensation and most importantly paved the way for the development of an assist-as-needed (AAN) control

strategy that encourages active patient participation.

5.1. Future work

Although the impedance control is working properly, this is just a starting point in order to develop a control that provides a more fluent and faster walking, thus more similar to a natural walking pattern.

A solution to obtain a motor pattern as natural as possible, is the development of a *finite state machine*(FSM) that defines different motion scenarios and logics to provide the desired assistance for patients [48].

The gait cycle is divided into different states: early stance, middle stance, late stance, swing flexion and swing extension. The states are connected in a sequential way and to enter or exit a state, conditions must be satisfied. Moreover, within a state, variables are set [49–51]. In the TWIN joint, for example, in each state there are specific values of k and θ_0 that realize a certain type of impedance. In order to pass from one state to another, a check of the joint angular positions and velocities is required.

In other words, the patient to move from one state to another must have the joint in a precise angular range, and once there, for the duration of that phase, the joint will work with specific impedance parameters.

So this project could focus on a logical diagram of this type and a FSM can be implemented in Simulink environment through the use of Stateflow It provides in fact a graphical language that includes state transition diagrams, flow charts, state transition tables, and truth tables. Stateflow can be used to see how models react to input signals, events, and time-based conditions.

This future implementation would greatly improve human-exoskeleton interaction.

Bibliography

- [1] World Health Organization. Spinal Cord Injury and Stroke. URL <https://www.who.int/news-room/fact-sheets/detail>. Available online.
- [2] Xing Chen et al. Improving the transparency of an exoskeleton knee joint based on the understanding of motor intent using energy kernel method of emg. *IEEE Transactions on Neural Systems and Rehabilitation Engineering*, 25(6):577–588, 2016.
- [3] Signe Brunnstrom. Motor testing procedures in hemiplegia: based on sequential recovery stages. *Physical therapy*, 46(4):357–375, 1966.
- [4] Riener Robert. Model-based development of neuroprostheses for paraplegic patients. *Philosophical Transactions of the Royal Society of London. Series B: Biological Sciences*, 354(1385):877–894, 1999.
- [5] R Reiner. Neurorehabilitation robotics and neuroprosthetics. *Neuroergonomics: the brain at work*, 2006.
- [6] David J Reinkensmeyer et al. *Neurorehabilitation technology*. Springer, 2016.
- [7] Joseph Hidler et al. Role of robotics in neurorehabilitation. *Topics in spinal cord injury rehabilitation*, 17(1):42–49, 2011.
- [8] Giovanni Morone et al. Robot-assisted gait training for stroke patients: current state of the art and perspectives of robotics. *Neuropsychiatric disease and treatment*, 13:1303, 2017.
- [9] Andrew Pennycott et al. Towards more effective robotic gait training for stroke rehabilitation: a review. *Journal of neuroengineering and rehabilitation*, 9(1):1–13, 2012.
- [10] BS Rupal et al. Lower limb exoskeletons: a brief review. In *Conference on mechanical engineering and technology (COMET-2016), IIT (BHU), Varanasi, India*, pages 130–140, 2016.

- [11] Daniel S Pamungkas et al. Overview: Types of lower limb exoskeletons. *Electronics*, 8(11):1283, 2019.
- [12] Bing Chen et al. Recent developments and challenges of lower extremity exoskeletons. *Journal of Orthopaedic Translation*, 5:26–37, 2016.
- [13] Wei Meng et al. Recent development of mechanisms and control strategies for robot-assisted lower limb rehabilitation. *Mechatronics*, 31:132–145, 2015.
- [14] Parker Hannifin Corporation. Indego. URL <http://www.indego.com/indego/en/research>. Available online.
- [15] Ekso Bionics. Ekso. URL <https://eksobionics.com/research>. Available online.
- [16] Argo Medical Technologies Ltd. Rewalk. URL <https://rewalk.com/resource-type/clinical-publication/>. Available online.
- [17] Luca Simoni et al. Friction modeling with temperature effects for industrial robot manipulators. In *2015 IEEE/RSJ international conference on intelligent robots and systems (IROS)*, pages 3524–3529. IEEE, 2015.
- [18] Mehrdad R Kermani et al. Friction compensation in low and high-reversal-velocity manipulators. In *IEEE International Conference on Robotics and Automation, 2004. Proceedings. ICRA'04. 2004*, volume 5, pages 4320–4325. IEEE, 2004.
- [19] Basilio Bona et al. Friction compensation in robotics: an overview. In *Proceedings of the 44th IEEE Conference on Decision and Control*, pages 4360–4367. IEEE, 2005.
- [20] Khairul Anam et al. Active exoskeleton control systems: State of the art. *Procedia Engineering*, 41:988–994, 2012.
- [21] Neville Hogan. Impedance control: An approach to manipulation. In *1984 American control conference*, pages 304–313. IEEE, 1984.
- [22] Paolo Rocco. Appunti del corso di robotica industriale. Dispense, Politecnico di Milano.
- [23] Christian Vassallo et al. Gait patterns generation based on basis functions interpolation for the twin lower-limb exoskeleton. In *2020 IEEE International Conference on Robotics and Automation (ICRA)*, pages 1778–1784. IEEE, 2020.
- [24] Matteo Laffranchi et al. User-centered design and development of the modular twin lower limb exoskeleton. *Frontiers in neurorobotics*, 15, 2021.

- [25] Entellion. CMX battery. URL <https://www.accutronics.co.uk/cm-x-series-batteries/>. Available online.
- [26] Texas Instrument. DRV8301 three-phase gate driver with dual current shunt amplifiers and buck regulator. Data-sheet.
- [27] Padmaraja Yedamale. Brushless DC (BLDC) motor fundamentals. *Microchip Technology Inc*, 20(1):3–15, 2003.
- [28] Maxon. EC 90 flat. Data-sheet.
- [29] Texas Instruments. Tiva™ TM4C1294NCPDT Microcontroller. Data-sheet.
- [30] Harmonic Drive AG. CSD-2A Component Sets. Data-sheet.
- [31] SEGGER Microcontroller GmbH & Co. J-Link/J-Trace User Guide. Data-sheet.
- [32] Stefano Maggi. Dispensa sul Controller Area Network. Dispense, Politecnico di Milano.
- [33] esd Electronics. CAN-USB. URL <https://esd.eu/en/products/can-usb-2>. Available online.
- [34] Fabian Just et al. Exoskeleton transparency: feed-forward compensation vs. disturbance observer. *at-Automatisierungstechnik*, 66(12):1014–1026, 2018.
- [35] Bharat Joshi et al. Modeling, simulation and implementation of brushed dc motor speed control using optical incremental encoder feedback. In *Proceedings of IOE Graduate Conference*, 2014.
- [36] Mirandola Stefano. *Elettrotecnica ed elettronica per Elettronica*. Zanichelli Editore spa, 2012.
- [37] Tegoeh Tjahjowidodo et al. Friction identification and compensation in a dc motor. *IFAC Proceedings Volumes*, 38(1):554–559, 2005.
- [38] Fabio Rocca. Fondamenti di elaborazione numerica dei segnali.
- [39] MathWorks Inc. 1-D Digital filter. URL <https://it.mathworks.com/help/matlab/ref/filter>. Available online.
- [40] Paolo Zunino. Appunti di metodi numerici. Dispense, Politecnico di Milano.
- [41] MathWorks Inc. Curve Fitting Toolbox. User’s guide.
- [42] MathWorks Inc. Rotational Friction. URL

<https://it.mathworks.com/help/physmod/simscape/ref/rotationalfriction.html>.
Available online.

- [43] Eclipse Foundation. Eclipse IDE. URL <https://www.eclipse.org/ide/>. Available online.
- [44] The Qt Company. Qt Creator. URL <https://www.qt.io/product/development-tools>. Available online.
- [45] MathWorks Inc. Linear Regression. URL <https://it.mathworks.com/help/matlab/data-analysis/linear-regression>. Available online.
- [46] Francesco Castelli Dezza. *Appunti di dinamica delle macchine e degli azionamenti elettrici*. Dispense, Politecnico di Milano.
- [47] TRINAMIC Motion Control. Trinamic drivers. URL <https://www.trinamic.com/products/>. Available online.
- [48] Dong Jin Hyun et al. Development of ankle-less active lower-limb exoskeleton controlled using finite leg function state machine. *International Journal of Precision Engineering and Manufacturing*, 18(6):803–811, 2017.
- [49] Shiqian Wang, Letian Wang, Cory Meijneke, Edwin Van Asseldonk, Thomas Hoellinger, Guy Cheron, Yuri Ivanenko, Valentina La Scaleia, Francesca Sylos-Labini, Marco Molinari, et al. Design and control of the mindwalker exoskeleton. *IEEE transactions on neural systems and rehabilitation engineering*, 23(2):277–286, 2014.
- [50] Prudhvi Tej Chinimilli et al. Automatic virtual impedance adaptation of a knee exoskeleton for personalized walking assistance. *Robotics and Autonomous Systems*, 114:66–76, 2019.
- [51] Letian Wang et al. Actively controlled lateral gait assistance in a lower limb exoskeleton. In *2013 IEEE/RSJ International Conference on Intelligent Robots and Systems*, pages 965–970. IEEE, 2013.

A | Appendix A

The following graphs represent how the duty-based transparency controller in TWIN works. Remember that the duty inside the torque controller is calculated according to the relation 2.1. Its graphical representation is shown in the Figures A.1 and A.2.

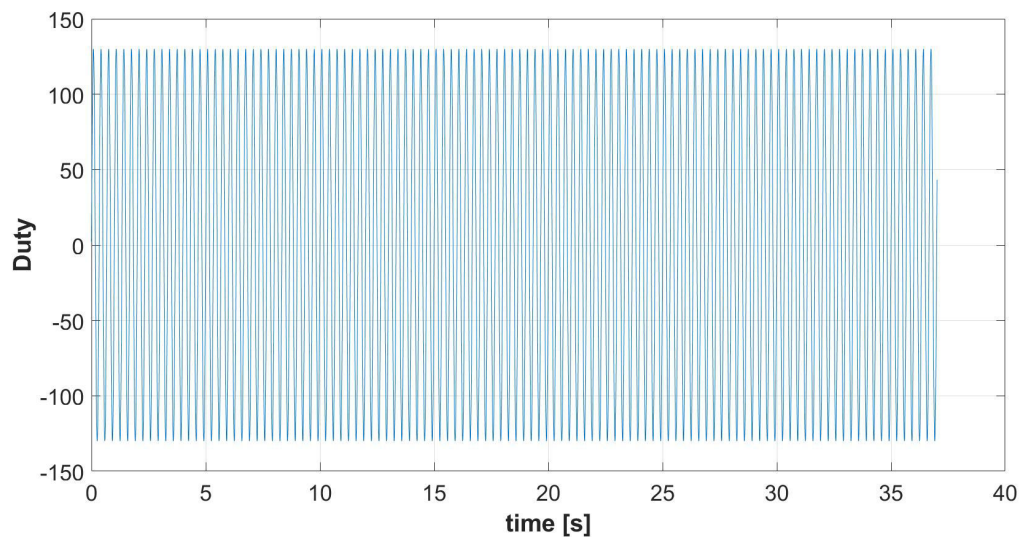


Figure A.1: Duty contribution for static friction, see equation 2.1a

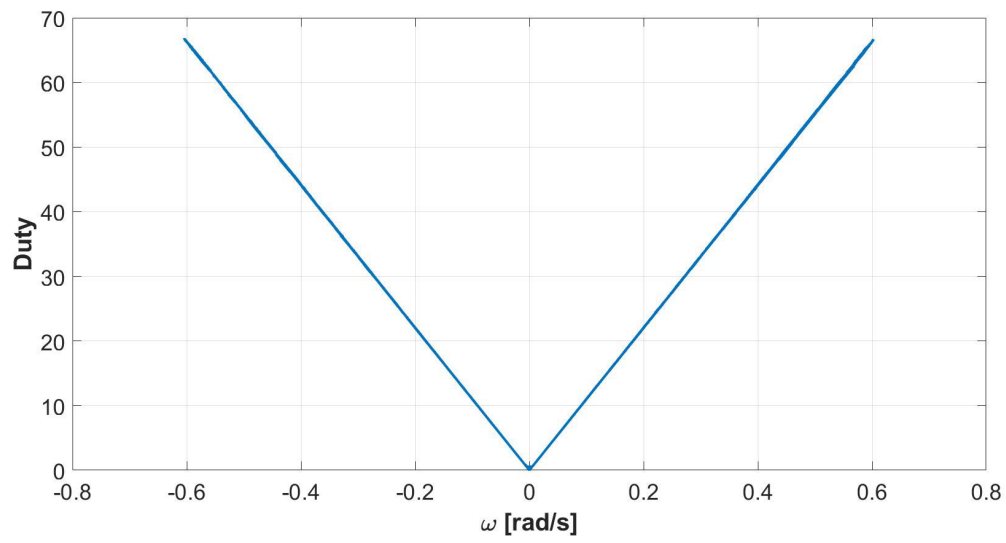


Figure A.2: Duty contribution for viscous frictions, see equation 2.1b

B | Appendix B

In this section results from the testing campaign are shown (only for knee joint by way of example). Remember that the load torque has been calculated according to the relation 2.8. This type of analysis was performed for each weight and the results are grouped into graphs showing the torque as a function of position, the position as a function of time, and the torque as a function of angular velocity.

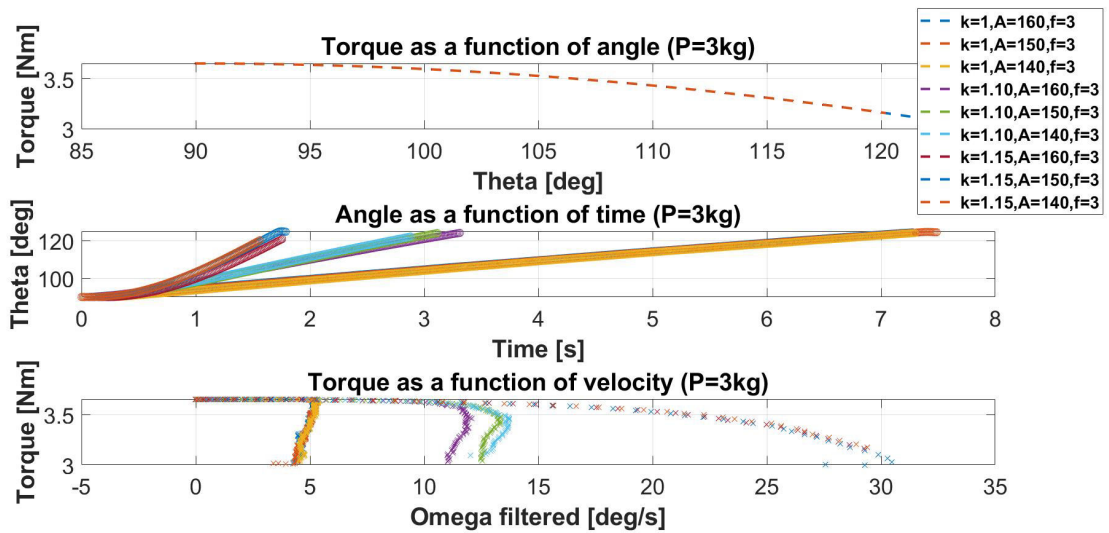


Figure B.1: Load torque for a weight of 3 kg

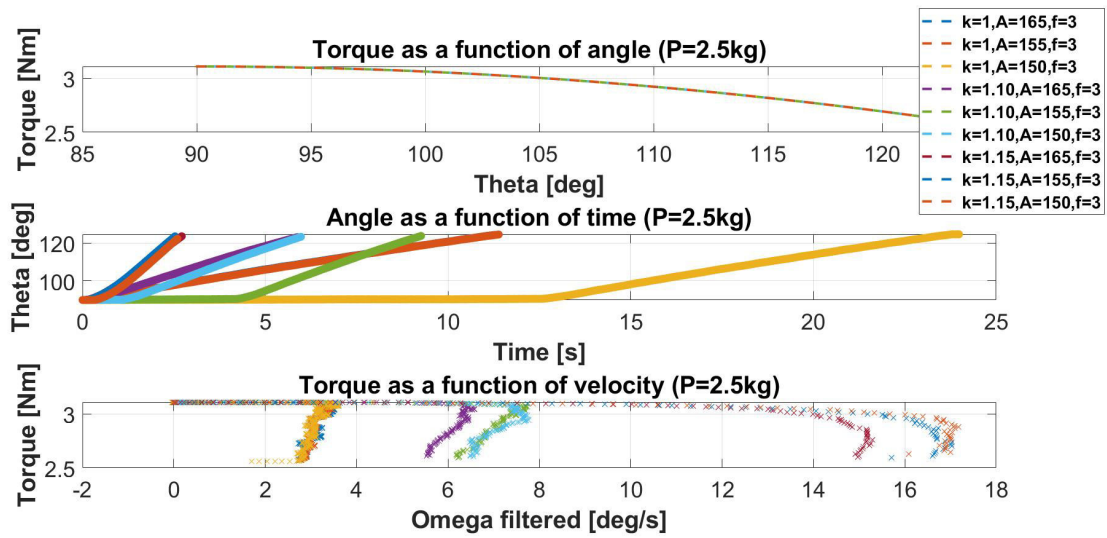


Figure B.2: Load torque for a weight of 2.5 kg

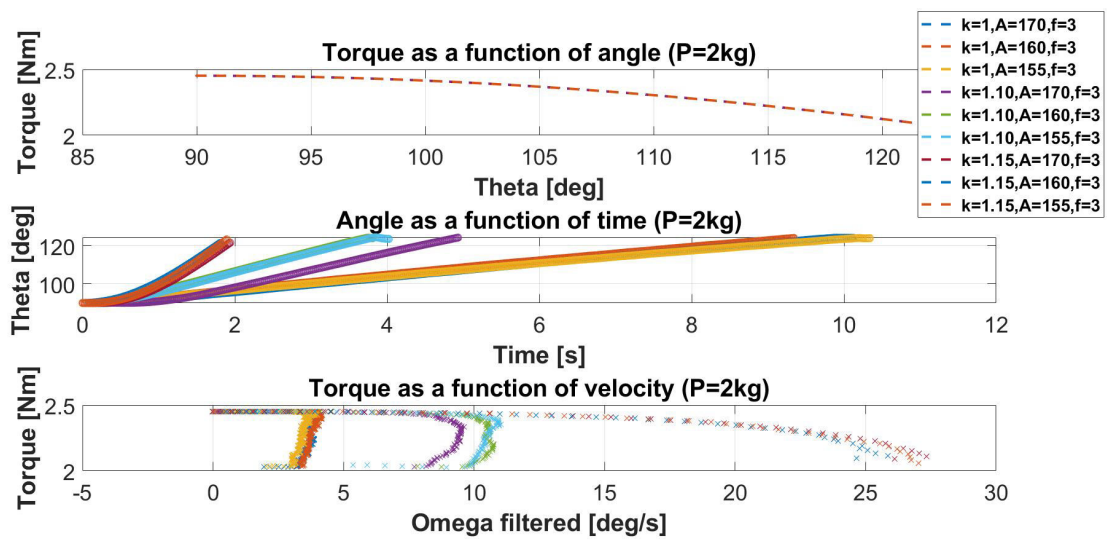


Figure B.3: Load torque for a weight of 2 kg

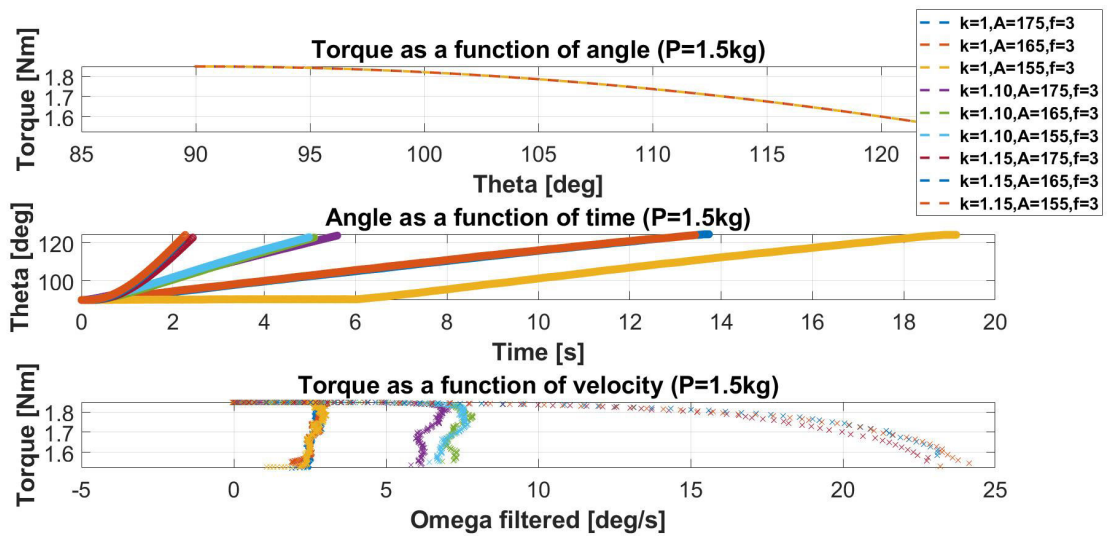


Figure B.4: Load torque for a weight of 1.5 kg

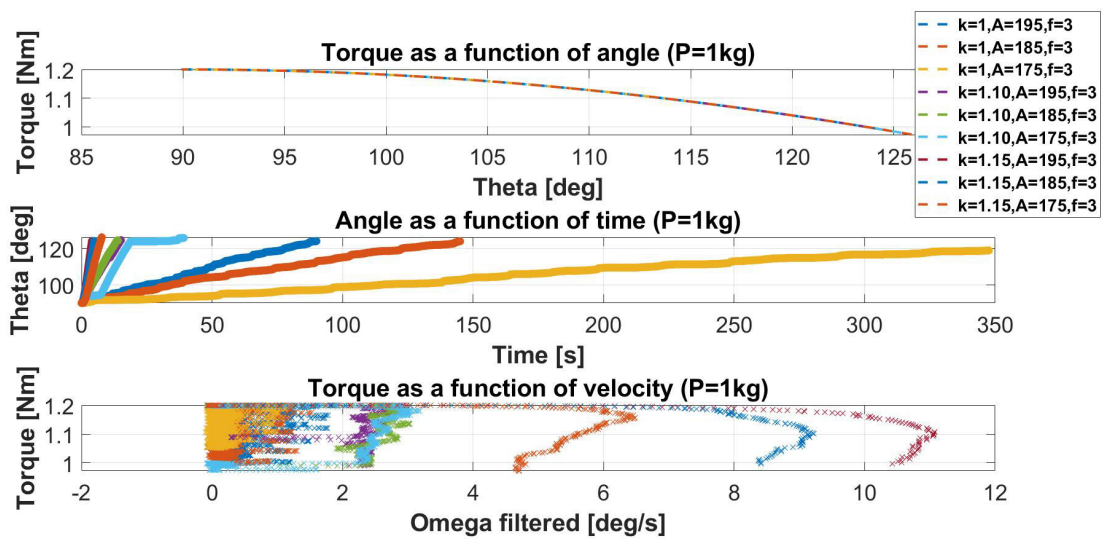


Figure B.5: Load torque for a weight of 1 kg

First, it can be seen that the position varies from 90° to 125° so, since the angular excursion is low, the arm does not vary a lot and therefore the torque does not change very much. This slight variation is appreciable in the first graphs of the various figures. Between one weight and another what changes is not the trend but the module that depends on the weight force.

In the graph of angle versus time the influence of K on the slope of the curves is evident. K affects the speed, in fact for high K the shaft reaches with less time the final position

of 125° . With a weight equal to 1kg and $K = 1$ the shaft takes too many seconds to reach the final position. Moreover the curves' trend results to be a piecewise linear curve, because during the test it often happened that the shaft in the descent phase blocked and took some instants to restart the movement, so the time to receive a sinusoid, then to overcome the static friction and to move again. For $K = 1.15$ and for high weights the curves show a remarkable improvement. With a focus on the first instants (see Figure B.6) the influence of A is evident. By varying the amplitude by 5 or 10, we can see how the shaft takes more or less time to overcome the static friction and to move. We must always keep in mind, however, that sometimes the shaft took longer to start moving because some gear teeth made more friction than others.

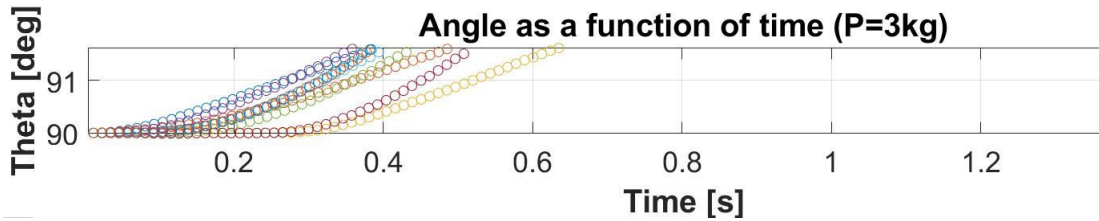


Figure B.6: Influence of the parameter A . This chart is a zoom on the initial instants of the B.1 second graph, so the legend is the same (not reported here because of space requirements)

Also in the graphs of torque versus angular velocity it is possible to see the considerable influence of K . For $K = 1.15$ the curve is much smoother without abrupt deviations. An acceleration of the shaft is appreciable, since the transmitted torque is greater than the resistant torque. It should be noted that where there are abrupt deviations indicating a sudden deceleration of the shaft, the reasons are that the shaft reached its final position, hitting the base of the test bench and decelerating, or the test was interrupted manually. Therefore, the points related to this deceleration are not to be considered for subsequent analysis. Another clarification: it is evident that as the weight increases, the curves are always less noisy. So it is true that K , A and f influence transparency, but it is also necessary that the weight force is not too low. To conclude, thanks to these tests we can see that the real difference in the duty-based transparency control is made by K , which is the value that actually allows transparency and acts once the minimum speed is exceeded. Amplitude and frequency help the joint to reach this minimum speed, overcoming the static friction and starting the movement of the joint.

List of Figures

1.1	Schematic of the human-exoskeleton cooperation system [12].	10
1.2	Indego exoskeleton	12
1.3	Ekso exoskeleton	13
1.4	ReWalk exoskeleton	15
1.5	Mass-spring-damper system	19
2.1	TWIN structure and wearability	22
2.2	Structural parts of TWIN	24
2.3	Internal structure of a TWIN joint	25
2.4	Braces	26
2.5	Logic structure of TWIN	27
2.6	Joint test bench	28
2.7	Schematic diagram of the joint test bench	29
2.8	Elements of the test bench	31
2.9	Joint-PC connections	33
2.10	Duty-based transparency controller	34
2.11	Motor-load system	35
2.12	Coulomb+viscous model in TWIN joints	36
2.13	Torque controller	37
2.14	Load torque acting on the joint	39
2.15	Experimental setup	40
2.16	Joint' torques	42
2.17	Rotational friction model	44
2.18	General impedance control	46
2.19	TWIN impedance controller	46
2.20	Linear stiffness	47
2.21	Leg test bench	49
3.1	Post-processing of the angular velocity	52
3.2	Knee friction compensation model	53

3.3	Hip friction compensation model	54
3.4	Hip and knee friction compensation models	55
3.5	Motor current values comparison	56
3.6	Impedance torque	57
3.7	Impedance torque with different friction compensations	58
A.1	Duty static contribution	69
A.2	Duty viscous contribution	70
B.1	Load torque for a wight of 3 kg	71
B.2	Load torque for a weight of 2.5 kg	72
B.3	Load torque for a weight of 2 kg	72
B.4	Load torque for a weight of 1.5 kg	73
B.5	Load torque for a weight of 1 kg	73
B.6	Influence of the parameter A	74

List of Tables

2.1	TWIN's specifications [24].	23
3.1	Models' parameters	55

Acknowledgements

I would like to thank Professor De Momi for giving me the opportunity to develop this project in a stimulating environment such as IIT.

I thank also the entire Rehab lab for their help during these months, but most of all for making this thesis experience an important educational experience.

In particular I want to thank Stefano and Christian for their help even on topics that initially were distant and incomprehensible to me. The knowledge I brought home thanks to you was fundamental.

I thank Federico infinitely for being a perfect and patient tutor since 2018. Having you by my side even in this challenging project made the experience enjoyable and challenging. Thank you for always believing in my capacities.

Finally, I thank Anna and Giulia, colleagues and friends who made the stay in Genoa extremely fun and who have always been supportive during these months.

